Reply to Reviewer:

General comments:

This study shows comparisons of MLT dynamics between the ground-based observations and the new reanalysis data which covers the mesosphere. The new analysis technique which could overcome data gap and uneven sampling in the observation is well introduced, although a setting of the vertical retrieval kernel should be carefully dis-cussed. The authors clearly describe the good performance of NAVGEM-HA reanalysis data in terms of climatology and the short-term response to the sudden stratospheric warming. The possible mechanisms for the short-term response of the semi-diurnal tides are also well discussed in Section 5. Since this paper shows many attractive observational/simulated results, the time-lag and/or the time scale of the short-term response of the semi-diurnal tides, in my opinion, should be a little more described in Section 4, which might be helpful for the discussion of the above mechanisms. In addition, the discussion section could be shortened by moving some sentences/paragraphs to the other sections. So, I would recommend publication of this paper only with some minor revisions described below.

General reply:

We thank the reviewer for his constructive and helpful comments about the submitted manuscript. We revised the manuscript according to his suggestions. However, as the second reviewer recommended a more extensive revision, the changes to the manuscript are in some paragraphs substantial. A point by point reply to each raised comment is given below.

Comment:

1. Page 4, line 18: It would be better to replace the sentence “The Rayleigh backscat-ter is . . . under the assumption of hydrostatic equilibrium” by a new one; “The temperature are calculated under the assumption of hydrostatic equilibrium from the Rayleigh backscatter which is proportional to the atmospheric air density.”

Reply: (Page: 5 line: 3)

We changed the sentence as suggested.

Comment:

2. Page 4, line 22: “only down to”→“only above” ??

Reply: (Page: 5 line: 6)

We followed the suggestion.

Comment:

3. Page 4, line 29: please delete “?”.

Reply: (Page: 5 line: 14)

There was a reference missing due to a mistake in the latex file. We cited Kuhl et la., 2013.

Comment:

4. Page 5, line 28: What is the advantage of the ASF compared with a wavelet technique such as S transform (Stockwell et al., 1996)?

Reply: (Page: 7 line: 29-)

We added a short paragraph discussing the pro and cons of both techniques.

The ASF technique aims, similar to the S-transform \citep{Stockwell:1996}, to infer spectral information of intermittent signals. However, the S-transform is based on wavelet techniques and, thus, takes all the pros and cons of these methods. The main benefits of the ASF are given in the error, the possibility to use unevenly sampled time series with data gaps and most importantly to apply individual constrains (in this study vertical wavelengths) to each fitted frequency component. Both methods should yield similar results for model data sets that obey the requirements mentioned above.

Comment:

5. The benefits of the ASF and a part of the discussion for the vertical kernel described in Section 5.1 would be better to be moved in Section 2 to shorten Section 5.

Reply: (Page: 7 line: 21-28)

We moved parts of section 5.1 to the ASF section and linked the new paragraph to this discussion.

Comment:

6. Page 6, lines 1-12: Please insert two references about gravity waves in MLT regions: Chen et al. (2013) to (Page 6, line 9), which shows a case study of observed gravity waves with the vertical wavelength of 22~23 km. Shibuya et al. (2017) to (Page 6,line 6). which shows a case study of gravity waves with the wave periods of quasi-12h (The climatological study of the above cases is discussed in Chen et al., 2016, JGR and Shibuya

and Sato, 2019, ACP, respectively, which I think need not to be introduced here).

Reply: (Page: 7 line: 13-16)

We added a short discussion of the first two publications into the paragraph. Both publications are interesting and highly relevant for this study. As the rather long vertical and horizontal wavelength, which are reported in both papers at such high latitudes brings new issues to the debate on how to separate a tide from a gravity at the polar regions. Further, considering She et al., 2016, who outlined that tidal waves satisfy the polarization relation for gravity waves.

Comment:

7. Page 7, lines 22: The altitudes of the wind reversal are quite different from the observations and the reanalysis data, which should be mention in the main text. The altitude of the wind reversal is quite important for the breaking condition of the upward propagating gravity waves.

Reply: (Page: 7 line: 13-16)

We added some sentences explicitly pointing at these differences at their relevance for gravity wave propagation and breaking. On the other side we have to mention that NAVGEM-HA winds and temperature fields are in much better agreement with the observation than many other GCM's perform at these altitudes. Even gravity wave resolving models seem to have difficulties to reproduce the observations in such details. Maybe such comparisons should become a benchmark to validate and cross-compare in climatological sense free running GCM's, reanalysis data sets and meteorological analysis (e.g. NAVGEM-HA).

Comment:

8. Page 8, lines 9: Why is the amplitude of the semi-diurnal tides in reanalysis data overestimated above the altitude of 90 km? I'm afraid that this point is not discussed in Section 5.

Reply: (Page: 5 line: 18-28)

We added a paragraph outlining the issue with the altitudes above 90 km. After removing the sponge layer from NAVGEM-HA and converting the geopotential altitudes to geodetic altitudes using WGS84 the uppermost trustworthy altitude is 92 km during winter and 90 km during summer. In fact, tidal amplitudes should not be interpreted beyond these altitudes. Our regridding up to 94 km led to an extrapolation of the tidal amplitudes, which was further enhanced due to the vertical regularization of the ASF. This is now clearly stated in the manuscript.

Comment:

9. Page 10, in Figure 3: Please add the explanation to the representation of a tidal phase (p12?).

Reply: (Figures 3,4,5,6,7 and 9,10)

We added an explanation of the labels to the figure caption.

Comment:

10. Page 10, line 9: Please mark the central date of the sudden stratospheric warming in the figures after Fig. 6.

Reply: (Figures 3,4,5,6,7,8 and 9,10,11,12,13)

We indicated the onset of the SSW for each figure using the definition from McCormack et al., 2017. The onset is given by a black vertical line.

Comment:

11. Page 10, line 12: Why does the data gap in the observation at Andenes exist near the central date of SSW? Is this related to the SSW?

Reply:

The Andenes MR radar had a technical problem and was off for some days. This happens frequently. Mostly due to icing of the antennas or strong winds, which significantly degrades the VSWR and triggers a shut-down of the transmitter. Whether this was related to the SSW is beyond our knowledge.

Comment:

12. Page 11, line 6 (CRITICAL): Please mention the time-lag between the central date of the SSW and the amplification of the semidiurnal tide both in the observation and the reanalysis data in Figs 6, 7, 9 and 10, respectively.

Reply:

We agree to the reviewer that the time-lag between the SSW and the onset of the enhancement of the semidiurnal tide is important. We are already preparing another study with more events to systematically look at this pattern and time scales. However, as the vertical propagation of the semidiurnal tide is mostly affected by the local(regional) air packages in the column around our measurement locations, the classical definition of a central day of a SSW seems to be not appropriate to measure the time-lag (e.g. the zonal wind reversal at 60°N). For different latitudes the zonal wind and the zonal wind reversal depend on the polar vortex position and its evolution, thus, we have to find another definition to measure the time lag.

If we define the max of the zonal wind reversal at a given latitude at 70 km altitude as central day, the time-lag is about 1-3 days. It takes 1 day for the onset of the tide amplification and 2-3 days to reach the maximum amplitude.

If we use the standard definition of the central day at 10 hPa and at 60°N, the time lag is between 3-6 days at Andenes and 2-3 days at Juliusruh.

Thus, the discussion of time delays and a potentially new definition of the central day at local coordinates would require a more detailed study, which is in preparation.

Comment:

13. Page 12, line 4: In Figure 8, the SW2 tidal amplitude seems to decrease after the central date of SSW below the altitude of 85 km? Such a decrease is not dominant in each localized point in NAVGEM-HA in Figs. 6 and 7. Why is this found only in the zonal mean?

Reply:

We were not aware of this feature so far. A detailed analysis is beyond the scope of the paper. However, there are two aspects that are relevant and need to be further disentangled. As shown in the appendix, there occur short and sudden enhancement of non-migrating tides before and after the SSW event (SW1, SW3), which might just be an artefact due to aliasing or a real excitation of both non-migrating tides modes. The local diagnostic only reveals a superposition of the migrating and non-migrating modes and, thus, depending on the phase behavior and the longitude of the observations, they might pick up only the positive interference of all tidal modes.

The second aspect are the planetary waves and the how the SSW affects the polar vortex. In the case of the SSW 2010, the polar vortex was clearly displaced to the European sector (see publications of Kodera et al., 2016), which is the sector of our observations. As a result the local diagnostic can look rather different with respect to the zonal mean. The planetary wave also has an effect on the amplitude of the tides can growth with altitude. Depending on the PW structure of wave numbers 1,2 and 3 the vertical propagation of tides is affected.

Comment:

14. Page 21, line 21-24: Please move the sentence “Atmospheric. . .” to Introduction.

Reply: (Page:3 line:17-29)

We moved the sentence to the introduction.

Comment:

15. Page 22, line 4-9: For the discussion of the amplification of the tides after the SSW, the time-lag of the amplification should be one of the key components. For example, the time-lag might be related to the vertical group velocity of the tides which propagate from the source region. Did the previous study discuss such a time-lag in their proposed mechanism?

Reply:

We thank the reviewer for making this comment. The vertical propagation of the tides is indeed a key element and, thus, the time lag between the SSW and the enhancement at least not in the context of the lunar tide. Only Forbes and Zhang (2012) mentioned the time delay between the central day and the semidiurnal tide amplification, which they then attributed to a lunar tide. However, given the dramatic change in the vertical wavelength of the semidiurnal tide from 50-60 km before the SSW to 200-300 km during a back after 3-5 days to 50/60 km indicates already that the vertical group speed is essential. We currently working on a more detailed analysis using a more extended dataset of NAVGEM-HA and observations. We now put more emphasis on this aspect throughout the manuscript. However, a more detailed study is in preparation with more data and events.

Comment:

16. Page 22, line 24: Moreoverr→Moverover.

Reply: (Page: 25 line:22)

Done.

Comment:

References:

Chen, C., Chu, X., McDonald, A. J., Vadas, S. L., Yu, Z., Fong, W., and Lu, X.: Inertia gravity waves in Antarctica: A case study using simultaneous lidar and radar measurements at McMurdo/Scott Base (77.8◦S, 166.7◦E). Journal of Geo-physical Research: Atmospheres, 118(7), 2794-2808, 2013.

Shibuya, R., Sato, K., Tsutsumi, M., Sato, T., Tomikawa,Y.,Nishimura, K., and Kohma, M.: Quasi-12 h inertia–gravity waves in the lower meso-sphere observed by the PANSY radar at Syowa Station (39.6_ E, 69.0_ S), Atmos. Chem. Phys., 17, 6455–6476, 2017

Reply:

We thank the reviewer for providing these additional references and included them at the suggested paragraph in the manuscript.

Comparative study between ground-based observations and NAVGEM-HA reanalysis data in the MLT region G. Stober et al.The authors present a study of tidal variability at altitudes of 75 to 110 km in the north-ern mid-to-high latitudes, emphasizing periods around stratospheric sudden warmings. They compare observations from a number of sources, most notably meteor radars, to NAVGEM-HA analyses. They also present a diagnostic tool called an adaptive spectral filter. It is not clear to me what the central purpose of the study is: is this a validation of the NAVGEM-HA reanalysis? is this a methodology paper introducing the adaptive spectral filter? Is this a science paper focusing on the variability of the tides around sudden warmings? I am not sure what the reader is supposed to take away from this paper

One symptom of this is that the bullet-point list of conclusions in the final section is vague. Several bullet points claim that the reanalyses are ’realistic’ and suitable for use as lower boundary conditions, but criteria for this claim are never discussed, and other validation papers cited seem to have drawn these conclusions already. Variations in the tide are attributed to variations in the ’wind patterns’ of the middle atmosphere but no evidence is provided to support this claim. The merits of the ASF methodology (e.g. error estimates) are touted but never used. And another ’holographic reconstruction’ methodology is used in the discussion section without ever being introduced.

I find the figures difficult to read, numerous, and not clearly organized with respect to the discussion, again my sense is that this is a symptom of the paper not having a clear purpose. Finally, the text of the manuscript is still rough around the edges, with incomplete sentences and missing references.

I’ve included a list of specific comments below. On the basis of the above comments it is my opinion that this manuscript should be substantially revised before it can be considered suitable for publication.

General Reply:

We thank the reviewer for his constructive comments to the submitted paper. We have revised the manuscript according to his suggestions and included new and the missing citations, added paragraphs providing some of the suggested information and restructured parts of the manuscript to provide a more consistent narrative.

NAVGEM-HA has not yet been validated in the climatological sense using independent ground base sensors. It is not worth to investigate the short time variability, if the seasonal climatology is not well-reproduced. The short-term variability and cross-validation of NAVGEM-HA fields with respect to specific waves is a new way to benchmark meteorological analysis systems, but is also tied to the methodology to extract the information, which is in the case the ASF technique. Although, we don't intent to focus on the method itself, it is necessary to provide essential information on the technique.

Finally, we present a detailed discussing of the tidal variability related to a highly relevant coupling process at the middle atmosphere (SSW) and its relation to alter in this case the semidiurnal tide. We discuss potential affects in the context of lunar tides, which provides an excellent example and demonstrate the potential of combining various local and global data sets to analysis effects on time scales that are hardly accessible with other methods at MLT altitudes.

In so far, we want to keep the general content of the paper, but did, as suggested, revise the structure and moved some paragraphs to get a better structure. We hope that the revised version satisfies the reviewers suggestions and comments.

Detailed answers are provided below for each comment.

Later there will be a tracked changes file uploaded. The red color labels removals, the blue color insertions.

Specific Comments:

Section 2:

Data and Model output:

Comment:

The periods for which data are available for each data source are not given. Neither are the 'analyzed periods' specified.

Reply: (Page: 3 line:3-4)

This information is provided in the section about mean winds.

Comment:

To what end have the temperature observations been included?

Reply:

There are only a few ground based temperature climatologies available. So far NAVGEM-HA was not yet compared to independent temperature observations. Satellite temperature measurements from MLS and SABER don't provide an independent data set due to the assimilation.

Comment:

Are the NAVGEM-HA outputs analyses or reanalyses? To what extent should the reader expect the tidal structures analyzed in this paper to be directly constrained by assimilated observations?

Reply:

NAVGEM-HA is a meteorological analysis, we removed through the manuscript the term reanalysis.

Comment:

What kind of sponge layer does the forecast model employ and over what levels does it act?

Reply: (Page: 5 line: 18-28)

We provide this information in section about NAVGEM-HA.

Comment:

There are missing citations in the first and third paragraph of section 2.3.

Reply:

The missing reference is now added.

Section 3: Diagnostics

Comment:

The details of the ASF are vague to the point that it is difficult to assess the validity of any of the results. For instance: how is the sliding window determined? What windows are in fact used? What is the purpose of the scaling factor? How is the vertical ’regularization’ carried out? If these details are given in previous studies this should be clearly stated, if they are novel they should be justified. No specifics are given about how planetary-scale waves are accounted.

Reply: (Page: 31 appendix A1)

We added the reference of previous developments of the ASF technique and how it was validated. Here we just mention the most important information of what was used in the ASF analysis. Further, we added a sentence outlined in more detail how the scaling factor is used to determine the window length.

We also add some figures in the appendix outlining how the technique works and about the error statistics. However, it will be critical for the readability of the submitted paper, if much more details about the ASF implementation are added to the paper.

The implementation of the ASF is in Fortran 77 and Matlab based on modified numerical recipes algorithms. Basically we generate for all times and altitudes Jacobian matrices, which can be written as one large block diagonal matrix (in development) or we keep each Jacobian (this is the current version) and create a cubic tensor (for each tidal frequency a separate layer due to the different window lengths). Then we solve each Jacobian and store the solutions into a vector. First for the diurnal tide. These solutions are used as regularization for the next layer with the Jacobian of the semidiurnal tide and so forth. Finally, we select all altitudes falling into the vertical averaging kernel and perform a weighted linear fit to all coefficients.

Below are two examples from the same day in 01st February 2010 observed at Juliusruh to visualize how the ASF reduce a potential contamination due to gravity waves with short vertical wavelengths. Filtering just in time domain would move energy from such gravity waves to the tidal energy budget. The plots also indicate that at the upper and lower edges the errors get very large, which is expected as we have no longer enough measurements to perform a statistical reliable regularization. The plots contain just the profiles obtained at a specific time at the day without temporal averaging in the case of the ASF. Therefore, the errorbars are scaled by 1/sqrt(n) to make them comparable to the temporal averaged values plotted as dashed line.

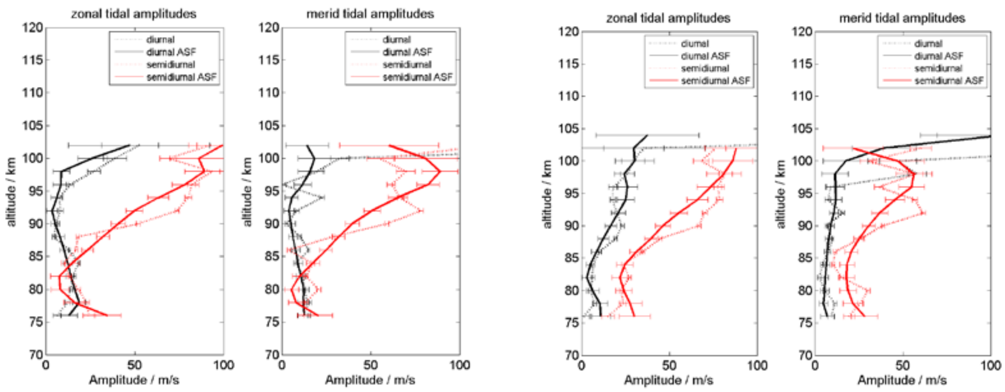

Comment:

Details of the ’holographic reconstruction’ methodology discussed in Fig. 12 should begiven in this section.

Reply: (Page: 25 line:2-16)

Holographic techniques are standard physical methods to derive radar parameters. However, we agree to the reviewer that it might be better to include a short paragraph describing how the hologram is obtained and used here in.

Section 4: Results

Comment:

Figure 1: What time periods have been used to create these figures? My reading of the figures is that the summertime reversal of the zonal winds from easterly to westerly occurs at higher altitudes in NAVGEM analyses than in the radar data, and that the southward meridional winds are not as strong. Is this the bias that is reiterated in the conclusions? Has this bias been noted in previous work?

Reply: (Page: 3 line:3-4)

We expanded the description of NAVGEM-HA, as the reviewer had already suggested this in the data and model section. This comparison is one of the first ones using summer-time NAVGEM-HA data for a comparison with independent ground based observations. The systematic differences in magnitude were not yet reported in a similar way in previous studies, although they were present there as well, but less obvious.

Comment:

Figure 2: The warm anomalies in NAVGEM-HA near 95 km are plausibly a sponge layer effect - one would need to know details of the sponge layer to assess this claim.

Reply: (Page: 5-6, lines 27-6(next page))

This point is also related to the model description section. We clearly remark to not use the summer-time data above 90 km due to sponge layer and extrapolation effects. The uppermost recommended usable pressure level in NAVGEM-HA after removing the sponge layer corresponds to a geometric altitude of 89/90 km at high and middle latitudes for the summer months. For the winter months the geometric altitude is between 91/92 km. Just focusing on the altitudes below 90 km, the agreement is much more reasonable compared to many other GCM’s.

Comment:

Figs. 3 to 5: The structure of the discussion (which discusses first observations then NAVGEM-HA) does not match the structure of the figures. More importantly the tidal amplitudes and phases in NAVGEM-HA do not look like close matches to observations to my mind. This would be a useful place to make use of the error propagation capabilities of the ASF methodology that are claimed as a benefit in later discussion.

Reply: (Page:5 line:18-28)

We moved some paragraphs sections to the model and data description sections to get better structure of the manuscript. Due to the required large size of the figures there is a clear mismatch between figure positions and text, however, this is very difficult to be fixed in the draft stage.

The mismatch of the tidal phases and amplitudes in NAVGEM-HA and the meteor radar at altitudes above 90 km is attributed to sponge layer and extrapolation effects during the gridding to geometric altitudes.

Comment:

Figs 4 to 6, 7 to 9: Again the structure of the figures and the discussion don’t match up.

Reply:

Due to the restructuring of some paragraphs this should have been improved.

Section 5:

Comment:

The merits of error propagation through the ASF methodology has not been demonstrated, nor has the benefits of the vertical resolution. I can see that these are both desirable features but no demonstration has been made of their value or correctness.

Reply:

The ASF methodology was already used in several publications before (Stober et al., 2017 (temporal ASF only), Stober et al., 2018a (gravity wave analysis using a MST radar), Stober et al., 2018b (retrieval of horizontally resolved meteor radar winds), Wilhelm et al. 2019 (mean tidal and wind climatologies as well as long term change analysis including significances based on full error propagation) and Baumgarten et al., 2019 (introduction and validation of 2D ASF using MERRA and lidar temperatures) as well as Pokhotelov et al. 2019 (cross comparison of GCM tides and meteor radar tidal climatologies). The benefit of wind retrieval errors and advanced statistical analysis including ASF filtering for spars data was demonstrated in Gudadze et al., 2019). So far substantial methodological problems were not raised by the other reviews and did not occur comparing the analysis to other climatologies.

The benefit of the error propagation is difficult to demonstrate. We propagate the error from the statistical uncertainties derived from the radar doppler velocity, which is based on the raw voltage statistics at the antennas, until the finally obtained wind or tidal component. The results presented herein are based making use of all these developments and we are sure there are differences, if we would redo all the analysis without such a weighting by the statistical uncertainties and the involved non-linear error models. If the results could be obtained without all the involved mathematics – there would be no benefit.

Please have a look on the following sequence of pictures. The left panel shows always the original parameter as zonal and meridional component, the right panels show the corresponding measurement uncertainties (here denoted error) in m/s.

Hourly winds computed using the algorithm presented in Stober et al., 2018.

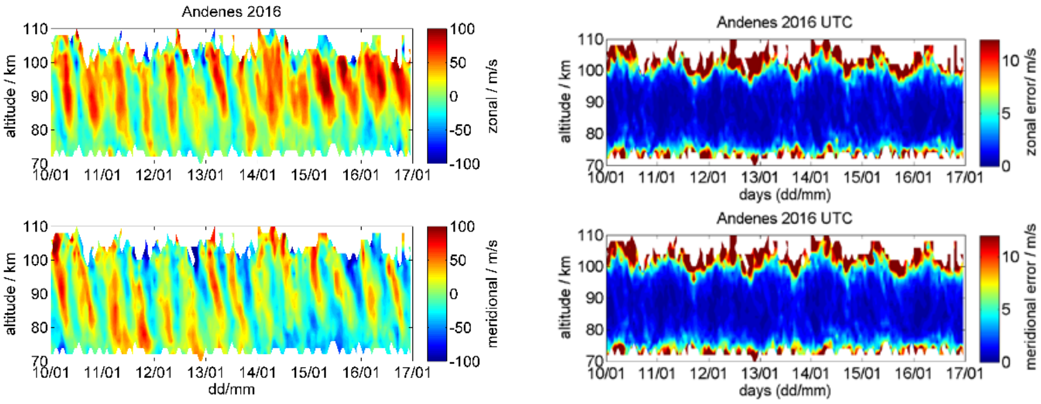

Daily mean winds after decomposing the time series with the ASF.

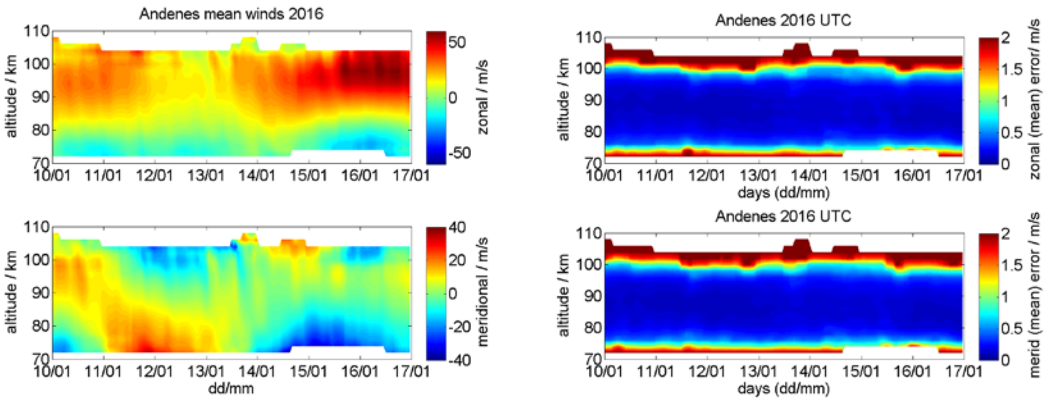

Diurnal tidal component

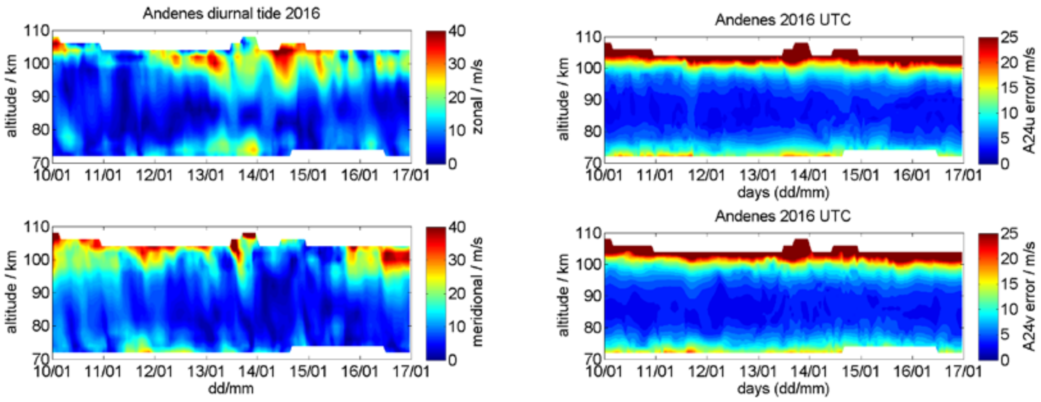

Semidiurnal component

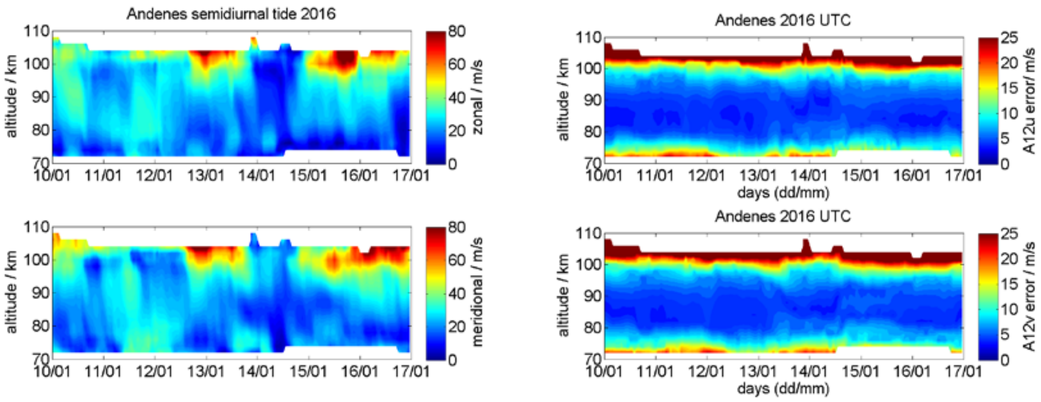

Comparison of hourly winds and reconstructed time series from mean winds and tides

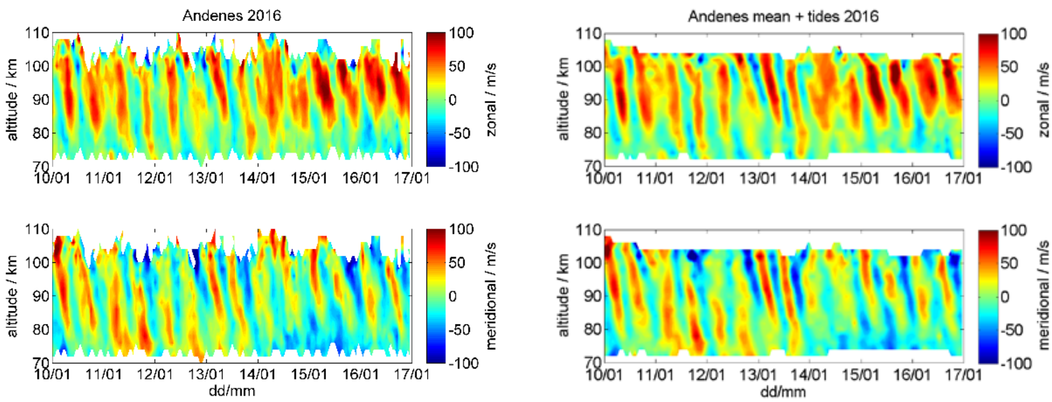

The reconstructed time series captures remarkably good the intermittent behavior of the observed tides and of the background mean winds.

Comment:

p22 lines 33-35: SSWs can perturb the middle atmosphere for months, as was the case in both the 2008-9 and 2012-3 events considered here.

Reply: (Page: 26 line:10-11)

The reviewer is correct. We rephrase this sentence to avoid confusion about the seasonal impact of SSW (Baldwin and Dunkerton, 2003 and many other publications). We now state that the wind reversal and cooling at the MLT last only for a few days during a SSW.

Comment:

Figure 12: What is the difference between the upper and lower panels? Also, the units for the period are wrong.

Reply:

We correct the unit and uploaded a new Figure including a vertical line indicating the onset of the SSW using the criteria presented in McCormack et al., 2017.

Comparative study between ground-based observations and NAVGEM-HA ~~reanalysis~~ analysis data in the MLT region

Gunter Stober[1,2], Kathrin Baumgarten[2], John P. McCormack[3], Peter Brown[4,5], and Jerry Czarnecki[2]

[1]Institute of Applied Physics, Microwave Physics, University of Bern, Bern, Switzerland
[2]Leibniz-Institute of Atmospheric Physics at the University of Rostock, Kühlungsborn, Germany
[3]Space Science Division, Naval Research Laboratory, Washington DC
[4]Dept. of Physics and Astronomy, University of Western Ontario, London, Ontario, Canada N6A 3K7
[5]Western Institute for Earth and Space Exploration, University of Western Ontario, London, Ontario, N6A 5B7, Canada

Correspondence: gunter.stober@iap.unibe.ch

Abstract. Atmospheric waves are a key driving mechanism for the circulation in the Earth's atmosphere. Such waves cover various spatial and temporal scales, e.g., planetary waves with periods of several days, atmospheric tides with periods of an integer fraction of a day and gravity waves with periods ranging from minutes to several hours. In particular, atmospheric tides gain large amplitudes at the Mesosphere/lower Thermosphere (MLT) region. Recently the day-to-day tidal variability as driver of the thermosphere-ionosphere system has become an emerging topic. Here we study the intermittent behavior of atmospheric tides by using meteor ~~radars~~ radar wind observations at altitudes of 75 – 110 km accompanied with lidar measurements. The observations are compared to meteorological analyses from NAVGEM-HA to infer how well the tidal variability on a daily to a seasonal basis is captured in the model. Therefore, a new diagnostic approach, a so-called adaptive spectral filter, is used to decompose the time series into a mean wind (zonal and meridional component) and temperature containing the planetary wave activity, atmospheric tides (diurnal, semi-diurnal and terdiurnal) as well as the gravity wave activity. By combining the local radar data with global ~~reanalysis~~ analysis fields, we extract the relative contribution of the migrating and non-migrating tides for the available data using a global version of the adaptive spectral filter. Our results indicate that the migrating semidiurnal (SW2) tide, which is the dominant mode at mid- and high latitudes at the MLT, shows a large seasonal variability in amplitude and phase. The comparison of NAVGEM-HA results ~~and the~~ with meteor radar observations demonstrate that the ~~reanalysis data reproduce rather consistent~~ meteorological analysis consistently reproduces the mean seasonal behavior as well as the day-to-day variability. This is especially obvious during sudden stratospheric warmings, where the SW2 tide shows a significant phase shift and amplitude modulation. These findings show the benefit of combining global high altitude data assimilation products with ground-based observations of the MLT region to better understand the tidal variability in the atmosphere.

1 Introduction

There is a growing need to understand the global wind field from the surface up to the lower thermosphere (0-100 km) and its day-to-day variability due to meteorological processes. Planetary waves and atmospheric tides are dominant drivers at the mesosphere and lower thermosphere (MLT) that provide a highly variable dynamical lower boundary to the thermospheric/ionospheric system, e.g. at the equatorial dynamo region at altitudes from 100 to 150 km (see, e.g. Akmaev, 2011, and references therein). The upward propagation of these drivers from their source regions near the surface into the MLT region is determined in large part by the global wind field. Accurate assessments of both daily and seasonal variability in winds and tidal modes has therefore become necessary for better understanding lower atmospheric forcing of the thermosphere/ionosphere system.

At mid- and polar latitudes planetary waves provide a significant contribution to the variability of the winter MLT and play a major role in vertical coupling processes between the different atmospheric layers. For example, during sudden stratospheric warmings (SSWs) (Matsuno, 1971; Andrews et al., 1987) the whole middle atmosphere (stratosphere/mesosphere) responds to sudden reversals of the zonal wind from eastward to westward and back to eastward accompanied by an increase of the stratospheric temperature and a mesospheric cooling (see, e.g. Chandran et al., 2014; Zülicke et al., 2018, , and references therin). SSWs are often studied using Global Circulation Models (GCMs), which are either free-running (e.g., GAIA, WACCM, KMCM, Jin et al. (2012); Liu et al. (2010); Becker (2017); Zülicke et al. (2018)) or nudged to reanalysis fields (e.g., SD-WACCM, Marsh (2011); Stray et al. (2015); Limpasuvan et al. (2016)). Manney et al. (2008, 2009) characterized the SSW in 2006 as a vortex displacement and the SSW in 2009 as a vortex splitting event making use of global satellite observations (MLS-Microwave Limb Sounder) and data assimilated reanalysis mostly at the stratosphere and lower mesosphere. Matthias et al. (2013) investigated the role of planetary waves in the evolution of vortex splitting and displacement events combining satellite data and ground-based observations.

Atmospheric tides are generated in the troposphere and stratosphere mostly through the absorption of sunlight by water vapor and ozone (e.g., Lindzen, 1979). They have been studied theoretically (e.g. Chapman and Lindzen, 1970; Forbes, 1982; Wang et al., 2016) and from observations (e.g. Portnyagin et al., 1993; Merzlyakov et al., 2009; Oberheide et al., 2009, 2011, and references therein) for decades. More recent studies analyzed the response of the semidiurnal tide during SSWs ~~(Conte et al., 2018)~~ using ground-based instruments and nudged GCM data ~~(HAMMONIA)~~ or investigated the relative importance and impact of the semidiurnal lunar tide during SSWs with TIME-GCM and WACCM (Pedatella et al., 2012; Pedatella and Maute, 2015). However, atmospheric tides propagate from their source region up to the MLT through a constantly varying altitude dependent wind field, which significantly modifies the phase of the tides, depending on their vertical wavelength, as well as the vertical wavelength itself.

In this study, we compare local meteor radar (MR) wind observations as well as lidar temperature measurements with meteorological analyses produced with NAVGEM-HA (Navy Global Environmental Model - High Altitude), a data assimilation and modeling system that extends from the surface to the lower thermosphere. NAVGEM-HA fields were availble from December 2009 to December 2010 and during the winter season 2012/13 starting in December 2012 until March 2013. Recent studies (Eckermann et al., 2018; McCormack et al., 2017) have presented initial cross-validation of the mesospheric winds from NAVGEM-HA for two winter seasons using worldwide distributed MR measurements. Here, we extend these initial comparisons to include seasonal mean winds (30-day median) from NAVGEM-HA and from three MRs at mid- to high latitudes for the year 2010. Time series of both NAVGEM-HA analysed winds and MR measurements are decomposed into daily mean winds, tides and GW residuals using a recently introduced analysis technique called adaptive spectral filter (ASF) ~~(Stober et al., 2017; Baumgarten and Stober, 2019)~~(Stober et al., 2017; Pokhotelov et al., 2018; Wilhelm et al., 2019; Baumgarten and Sto . This technique is designed to extract daily mean winds and tidal variations on a day-to-day basis. In addition to MR measurements, we also present the first comparison between midlatitude temperature observations from a resonance lidar and NAVGEM-HA analysed temperatures for the 2010 period. Finally, we present a detailed comparison of two SSWs in 2009/10 and 2012/13 and outline how the semidiurnal tide responds to changes in the background wind concerning the tidal phase and amplitude. Overall, the results of these comparisons show very good agreement between NAVGEM-HA analysed winds and MR observations, highlighting the utility of combining global high altitude data assimilation products with ground-based observations of the MLT to better understand tidal variability over daily to seasonal time scales.

Further, we present a cross-comparison of mean winds and semidiurnal tidal day-to-day variability during two SSW events. Such short time variations are essential for the understanding of the forcing from below of the thermosphere and ionosphere (Liu, 2016). Meteorological analysis data, such as NAVGEM-HA, provide a much more realistic forcing of the upper atmosphere due to tides and mean winds compared to current versions of other comprehensive models. Chandran and Collins (2014) investigated SSW events using WACCM-SD nudged with reanalysis fields from the GEOS-5.2 reanalysis system up to an altitude of about 40 km. However, at altitudes above 70-80 km the nudged model started to substantially deviate from the observed wind climatologies (Wilhelm et al., 2019). In particular, the nudged model showed a wind reversal from eastward to westwards winds between 70-80 km, which is not confirmed from the wind climatologies. Such reversal of the zonal wind can be also found in other comprehensive models or mechanistic models (Smith, 2012; Becker, 2012). Liu (2016) shows a comparison among several GCMs indicating that there are substantial deviations at the mesosphere and upper atmosphere, although each of the GCMs was nudged up to the lower stratosphere (see also Pedatella et al. (2014) for more details). Only the GAIA model (Jin et al., 2012; Liu et al., 2014) showed during winter eastward winds at the MLT.
Therefore, the paper is structured as follows. First, we describe the observations for winds and temperatures in the MLT region and the corresponding ~~reanalysis~~ meteorological analysis data in Section 2. ~~In~~ Section 3 ~~a~~ provides detailed explanation of the methodology used for the data analysis~~is given~~. Section 4 presents the results for the climatology, comparing mean winds simultaneously seen in the meteor radar data at different locations with the NAVGEM-HA ~~reanalysis~~ analysis data accompanied with available temperature measurements from a resonance lidar at one mid-latitude location. The results are also discussed for

the semidiurnal tide for the whole year as well as during the winter season in 2010 and 2013 in Section 5. Finally, the findings are summarized and a conclusion is given in Section 6.

2 Data description

2.1 Wind observations

In this study, we compare the 3-hourly global synoptic wind and temperature analyses from NAVGEM-HA with meteor radar observations collected at three different latitudes in Andenes (69° N, 11° E) in Norway, Juliusruh (54.3° N, 13° E) in Germany and Tavistock (CMOR- Canadian Meteor Orbit Radar) (43.2° N, 80.7° W) in Canada. All three meteor radars use the same software as described in Hocking et al. (2001). All systems were almost continuously in operation for the analyzed periods. Only the Andenes system shows some data gaps, mainly due to the more extreme weather conditions in Northern Norway, which caused some damage to the antennas and from time to time a power outage. A more detailed description of the CMOR radar can be found in Brown et al. (2008). A summary of the Juliusruh and Andenes MR is found in Stober et al. (2012) and Wilhelm et al. (2017).

MLT winds are obtained with a temporal resolution of 1 hour and a vertical resolution of 2 km using the wind retrieval algorithm as presented in Stober et al. (2018), which is a further development of the wind analysis presented in Hocking et al. (2001). The wind analysis contains a full error propagation of the statistical uncertainties and a physical error model based on the vertical and temporal shear as spatio-temporal Laplace filter for each wind component. Contrary to many other meteor radar wind analysis, the algorithm also solves for the vertical wind velocity. The obtained mean vertical velocities show values of a few cm/s and are mainly used as quality control for successful convergence of the wind fit. In the present study, we use 4 meteors as a minimum for a successful wind fit.

2.2 Temperature observations

At Kühlungsborn (54° N, 12° E), around 118 km southwest of the meteor radar at Juliusruh, a resonance lidar was in operation until 2012 to derive temperatures in the MLT region. The potassium lidar measures the Doppler broadening of the 770 nm potassium D1 resonance line by scanning with a narrow band Alexandrite ring laser. The system is fully daylight capable. Further details can be found in von Zahn and Höffner (1996); Fricke-Begemann et al. (2002).

The ~~temperatures are derived between approximately~~ extent of the potassium layer in the atmosphere limits the range of heights at which temperatures can be determined. In this work, temperatures are determined for heights between 80 and 105 ~~kmdepending on the extension of the potassium layer~~km. The integration time of the data used here is 1 h with a shift of 15 min. The vertical resolution is 1 km. In addition to the resonance lidar, also a Rayleigh-Mie-Raman (RMR) lidar is operated during the night at the same location until 2013. This lidar used the second harmonic output of a Nd:YAG laser at 532 nm. The ~~Rayleigh backscatter is proportional to the atmospheric air density from which the~~ temperatures are calculated under the assumption of hydrostatic equilibrium from the Rayleigh backscatter which is proportional to the atmospheric air density (Hauchecorne and Chanin, 1980). The initial temperature value for integration is taken from the resonance lidar (Alpers et al., 2004). The temperatures from the RMR lidar cover an altitude range between 22 and 90 km. But as the focus of this study is on the MLT region, we use these temperatures only ~~down to~~ above 70 km. Here, daily mean temperatures as a composite between 2003 and 2012 are used to describe the mean temperature field during the year in the MLT region. A full description of the seasonal variation has been published in Gerding et al. (2008).

2.3 NAVGEM-HA meteorological analyses

NAVGEM-HA is a high-altitude numerical weather prediction (NWP) system extending from the surface to ∼116 km altitude that provides atmospheric winds, temperatures and constituent information. It is based on the operational system described in Hogan et al. (2014), which combines the NAVGEM global spectral forecast model with a hybrid four-dimensional variational (4DVAR) data assimilation algorithm Kuhl et al. (2013).

In addition to standard operational meteorological observations in the troposphere and stratosphere, NAVGEM-HA assimilates satellite-based observations of temperature, ozone and water vapor in the stratosphere, mesosphere and lower thermosphere (McCormack et al., 2017). The NAVGEM-HA output is on a 1° latitude and longitude grid, respectively. The temporal resolution of the data output fields is 3 hours. NAVGEM-HA uses a fixed top level pressure of $6 \cdot 10^{-5}$ hPa (e.g., McCormack et al., 2017; Ec , which corresponds to an approximate altitude of 116 km. However, at the upper three model levels, an enhanced diffusion is applied to reduce the effects of wave reflection. These layers effectively act as a "sponge layer" and should not be included in the data analysis. The NOGAPS-ALPHA model incorporates implicit fourth-order horizontal diffusion of vorticity, divergence, and virtual potential temperature to suppress growth of unrealistic variances near the truncation scale, as described in McCormack et al. (2015) . Default values for the diffusion result in an effective e-folding time of 24 hours at the highest wavenumber (here T119). In the top 3 model levels the diffusion is ramped up to produce an effective e-folding of 2 hours at the top level. In the 74-level version of NAVGEM-HA used in this study, this region of enhanced diffusion (sponge layer) covers levels with $p <$ 1.e-3 hPa or 95 km in pressure-altitude.

McCormack et al. (2017) used for the initial validation geometric altitudes up to 95 km for the mean winds and a maximum altitude of 90 km for the wave analysis. For comparison with the ground-based instruments, vertical profiles of NAVGEM-HA analyzed winds and temperatures are converted from the model vertical grid in geopotential altitude to a geometric altitude grid as done in Eckermann et al. (2009). The vertical resolution decreases with ~~higher~~ increasing altitude and is 3-5 km between 80 and 100 km. To date, NAVGEM-HA winds and tides have been shown to be in good agreement with ground-based MR observations, as reported in McCormack et al. (2017)~~and~~ , Eckermann et al. (2018), and Laskar et al. (2019), and with independent satellite-based wind observations as reported in Dhadly et al. (2018).

In this study we use a fixed geometric altitude grid (based on the World Geodetic System 84 model) with a maximum altitude of 94 km and 2 km vertical resolution at the MLT to match the meteor radar data. We convert the geopotential altitudes of NAVGEM-HA to geometric altitudes. However, we have to note that the geopotential altitude of the highest model level , after removing the sponge layer, has a geometric altitude between 92 to 89 km. As a consequence tidal amplitudes above 90 km altitude should not be considered as geophysical and are caused by the extrapolation to the geometric altitude grid and sponge layer effects. Further, the vertical constraint implemented in the ASF amplifies this effect even more.

3 Local and global diagnostics

One of the challenges comparing different data sets is the use of a common diagnostic to ensure that all observations and the reanalysis meteorological analysis data are treated in the same way. In particular, observational data can be more difficult to be analyzed analyze due to data gaps or uneven temporal sampling. Atmospheric tidal and planetary wave amplitudes are often obtained from Fourier based techniques (e.g. Stockwell et al., 1996; Torrence and Compo, 1998)or for . In the case of unevenly sampled data (Lomb, 1976)Lomb-Scargle periodigrams are used Lomb (1976); Scargle (1982), which provide a amplitude/power spectrum and a significance level, but without a phase information. For observational data, it is also very common to derive the tidal information of amplitude and phase with a least-square fit (Lima et al., 2007) or by a multiple regression analysis assuming, for instance, a circular polarization for the semidiurnal tide (Jacobi et al., 2008).

A commonly used approach to extracted extract tides is a harmonic analysis:

$$u,v,T = u_0,v_0,T_0 + \sum_{n=1}^{3} a_n \sin(\frac{2\pi}{P_n}\cdot t) + b_n \cos(\frac{2\pi}{P_n}\cdot t) \quad ; \qquad (1)$$

here u,v,T are the zonal, the meridional wind and the temperature, a_n and b_n are the tidal Fourier coefficients, $P_n = 24,12,8$ stands for the tidal periods in hours and t is the time of the observation either in UTC or local time, whatever is preferred. Harmonic tidal analysis work well for time series of several days or months, but assumes a constant mean background wind, tidal amplitude, and phase for the selected period. Recent studies of mean winds and tides using meteor radarand lidar , lidar and satellite observations indicate that tides have a fairly intermittent amplitude and phase character (Stober et al., 2017; Baumgarten et al., 2018; Conte et al., 2018; Baumgarten and Stober, 2019)(Stober et al., 2017; Baumgarten et al., 20
.

The adaptive spectral filter (ASF) aims to be a simple and general diagnostic to decompose time series in 1-D (temporal filter) (Stober et al., 2017) or 2-D (temporal-spatial filter) (Baumgarten and Stober, 2019). The technique is based on least-squares and, hence, applicable to unevenly sampled data and no additional zero-padding needs to be applied for data gaps as long as sufficient observations are available in the remaining adapted time window. Another benefit of the least-squares implementation is given in the error propagation to the derived quantities through the covariance matrix. The term adaptive 'adaptive' in this context is relates, similar to the wavelet technique, in that the window length scales with adapts to the number of wave cycles for each frequency component that are fitted. The MR and NAVGEM-HA time series are decomposed into daily mean winds, diurnal tide, semidiurnal tide, terdiurnal tide and gravity wave residuum using the ASF.

The ASF uses a sliding window and fits each tidal component applying a scaling factor of 1.3 accounting for the number of wave cycles and no de-trending is applied. The scaling factor determines the window length that is used for the fitting for each frequency component. Here we applied a window length of 31 hours for the diurnal tide, whereas the semidiurnal tide is determined using a 16 hour window and so forth for the terdiurnal tide. At first, the daily mean wind and the diurnal tidal (amplitude and phase) components are determined considering also a potential semidiurnal and terdiurnal tide. In the next step, the semidiurnal tide is fitted using a regularization by the previously determined daily mean wind and diurnal tide and adapting the window length. The same procedure is repeated for the terdiurnal tide respectively. Due to the short window length, the bandwidth for each tidal component is rather wide and may also include some gravity wave contributions. It turns out that just applying temporal filtering leads to some contamination of the obtained tidal amplitudes and phases due to inertial gravity waves with short (less than 10 km) vertical wavelengths (see appendix A). However, there are also some studies from polar latitudes using lidar and radar observations from McMurdo/Scott base (77.8°S, 166.7°E) and from Syowa Station (39.6°E, 69.0°S) indicating the presence of gravity waves with vertical wavelengths of 22-23 km Chen et al. (2013) or periods close to the semidiurnal tide Shibuya et al. (2017). However, Davis et al. (2013) has shown that the diurnal and semidiurnal tide typically has vertical wavelengths larger than 20 km. Hence, we constrain our tidal amplitudes and phases by assuming that the phase of the diurnal and semidiurnal tide only gradually change with altitude using a 16 km vertical retrieval kernel. The mean winds are constrained by a 10 km vertical retrieval kernel to avoid issues during the summer wind reversal from westward winds to eastward winds.

Atmospheric tides are a major driver of the short term variability of the lower thermosphere/ionosphere. The developed ASF technique provides a new tool to decompose time series to assess this short term variability from local and global data sets and allows a unified data analysis from observations and models or meteorological analysis such as NAVGEM-HA. The benefits of the method are:

- data can contain data gaps (gaps have to be shorter than adapted window length)
- applicable to unevenly sampled time series
- full error propagation through covariance matrices
- individual vertical regularization for each atmospheric parameter

The ASF technique aims ,similar to the S-transform (Stockwell et al., 1996), to infer spectral information of intermittent signals. However, the S-transform is based on wavelet techniques and, thus, takes all the pros and cons of these methods. The main benefits of the ASF are given in the error, the possibility to use unevenly sampled time series with data gaps and most importantly to apply individual constrains to each fitted frequency component. Both methods should yield similar results for model data sets that obey the requirements mentioned above e.g. meteorological analysis like NAVGEM-HA (McCormack et al., 2017).

Since NAVGEM-HA produces global wind and temperature fields, we can extract tides as global waves and separate migrating and non-migrating tidal modes. Migrating tides are the DW1 (diurnal westward wave number 1), SW2 (semidiurnal westward wave number 2) and TW3 (terdiurnal westward wave number 3); all other tidal modes are non-migrating tidal components (e.g., Forbes et al., 2008; Miyoshi et al., 2017, and references therin). The migrating and non-migrating tidal components are obtained using the following function;

$$u,v,T = u_0,v_0,T_0 + \sum_{s=-3}^{3}\sum_{i=1}^{3}\Big(a_{si}\cdot\sin(s\cdot\lambda - \frac{2\pi}{P_i}\cdot t) + b_{si}\cdot\cos(s\cdot\lambda - \frac{2\pi}{P_i}\cdot t)\Big) + further\ waves \quad , \tag{2}$$

where s is the zonal wave number (negative eastward, positive westward), λ denotes the longitude at a fixed latitude circle, P_i are the periods of the diurnal, semidiurnal and terdiurnal tide and a_{si} and b_{si} are the Fourier coefficients for each wave number s and period P_i. The zonal mean zonal and meridional wind and the zonal mean temperature are given by u_0, v_0, T_0. The function also includes longer period waves such as the quasi two day wave (QTDW) with wave number s=1,2,3 and stationary planetary waves with wave number s=1,2,~~3.~~3 (Baumgarten and Stober, 2019; Schranz et al., 2019).

Daily mean tides for all the components are obtained by using a 3-day window around a central day, which is sufficient to still see some day-to-day variability and to determine potential phase drifts of each tidal component. The global tidal phase for all tidal components is referenced to the Prime meridian (Greenwich). Although NAVGEM-HA provides validated wind and temperature products up to ∼94 km altitude, we focus our comparison to the MLT region and mostly to the available MR observations. A detailed discussion of the QTDW or planetary waves is beyond the scope of this paper and we leave these for other studies.

4 Results

In the first two parts of the results, we show the mean state of the atmosphere during the year in the MLT region using winds and temperatures from observations and NAVGEM-HA data. Next, the seasonal variation of the semidiurnal tidal component derived with the adaptive spectral filter is presented for each location. In addition to this, the analysis is also done for two examples of sudden stratospheric warming in the winter 2009/2010 and 2012/2013 to determine how well the observed variations in the MLT winds correspond to the NAVGEM-HA ~~reanalysis~~ analysis data as well as to determine the day-to-day variability of the semidiurnal tide.

4.1 Mean winds

Fig. 1 shows the time variation of the zonal and meridional winds at the three locations Andenes, Juliusruh and Tavistock, from hourly meteor radar observations (left column), and the corresponding 3-hourly NAVGEM analyzed winds (center column) for the same location and each latitude as zonal mean values (right column). Daily mean winds are calculated and small scale variations such as tides and gravity waves are ~~effectively removed~~ removed by the adaptive spectral filter and planetary waves are effectively filtered using a 30-day running median. The climatologies are based on the same time periods for MR winds and NAVGEM-HA and include December 2009 until December 2010 with periodic boundary conditions. In general, there is

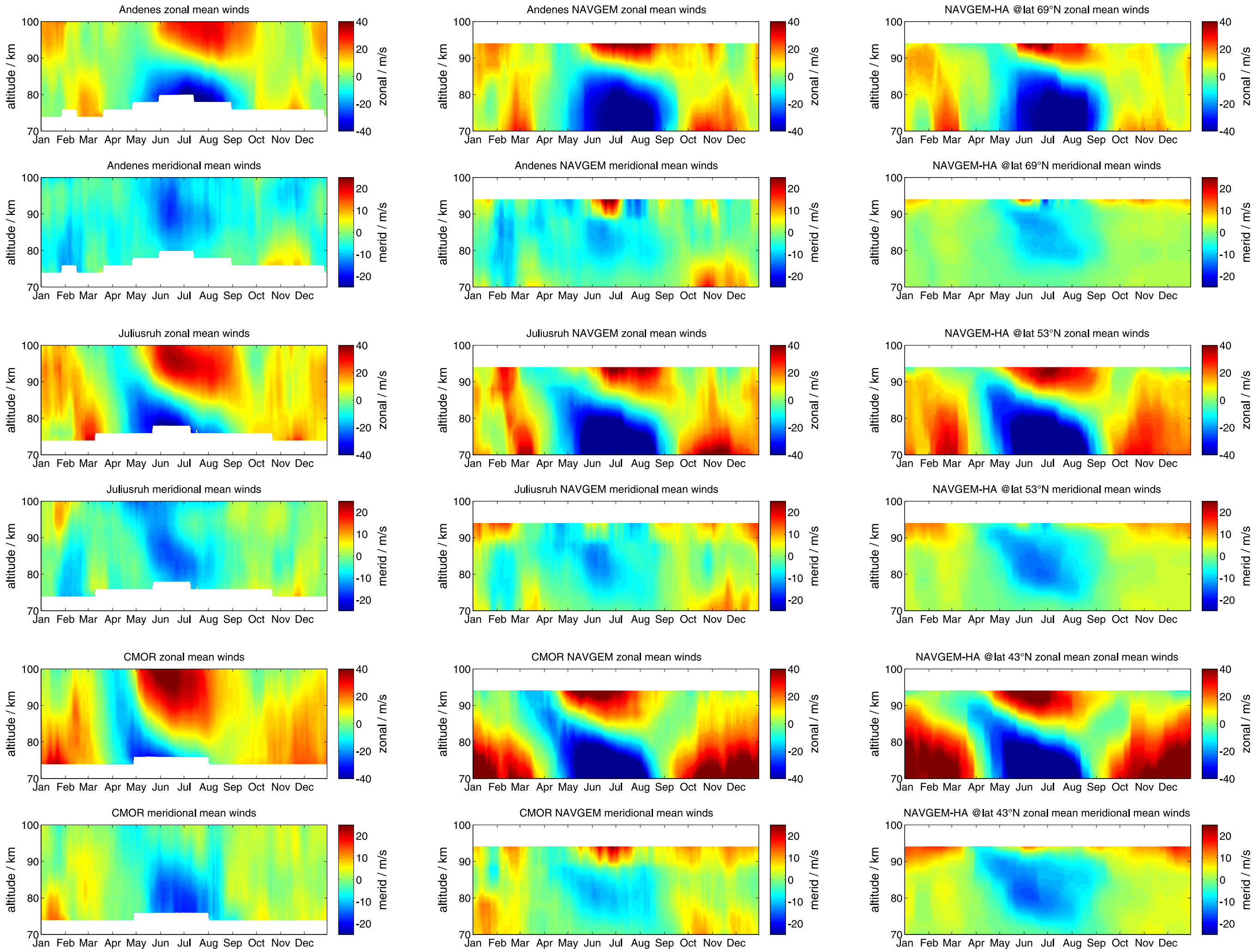

Figure 1. Comparison of mean winds above Andenes, Juliusruh and Tavistock (CMOR) using a 30-day running median with periodic boundary condition using the same dates for NAVGEM-HA and the meteor radar observations. The left panel shows the meteor radar observations. The central panel shows the NAVGEM-HA ~~reanalysis~~ analysis fields for the same locations and periods. The right panel displays the zonal mean zonal and meridional winds for each latitude.

a good agreement of the seasonal wind pattern between the meteor radar wind observations and the ~~reanalysis~~ NAVGEM-HA data. At all three locations, the zonal wind observations show the typical eastward directed winds in winter and the prominent wind reversal in spring.

During summer, a strong transition between westward and eastward winds occurs between 80 and 90 km altitude. The transition height decreases from high to midlatitudes. Above 90 km altitude, the eastward jet reaches wind velocities of about 40 m/s for all stations. The meridional winds during winter are typically northward~~directed~~, while they are southward ~~directed~~ during the summer. Similar behavior is seen in the NAVGEM-HA ~~reanalysis~~ analysis data, but here ~~,~~ the magnitude of the winds is to some extent larger compared to the meteor radar observations. Although the general morphology of the seasonal pattern is well captured in NAVGEM-HA, there are some differences in the wind reversal altitudes in summer in both wind components, which would affect the gravity wave breaking altitudes and, hence, the altitude of the resulting momentum deposition.

Furthermore, the altitude where the zonal wind reverses during summer decreases not as much with latitude as indicated from the meteor radar observations for the different locations. Some differences occur between the NAVGEM-HA locally analyzed winds compared to the zonal averaged NAVGEM-HA analyzed winds for each latitude of the meteor radar stations. Short-term variations during winter are much more visible in the locally analyzed winds, this is especially for the meridional wind the case.

4.2 Mean temperatures

A similar comparison to the NAVGEM-HA temperature field is done using a co-located potassium lidar at Kühlungsborn. The composite daily mean temperatures ~~as composite~~ over the years 2003-2012 from the lidar are shown in Fig. 2 together with the NAVGEM-HA analyzed temperatures between 2009 and 2010. Both data sets show the same seasonal temperature pattern with the lowest temperatures during summer. The mesopause, where the lowest temperatures occur during the year, is estimated from the lidar data at around 88 km in summer and just above 100 km in winter. For the NAVGEM-HA analyzed temperatures the altitude of the mesopause is in nearly the same altitude range. Even the magnitude of both temperatures is in very good agreement with each other. Only the temperatures observed by lidar around 70 km are higher compared to the NAVGEM-HA data. At the upper edge of the NAVGEM-HA data, there is also a temperature enhancement during summer, which is not seen in the lidar data.

4.3 Semidiurnal tides

In this section, we investigate the seasonal variation of the semidiurnal wind tide based on the calculation with the adaptive spectral filter. This component is the most dominant tidal component seen in the MLT region (Chapman and Lindzen, 1970). The results for the semidiurnal tidal amplitude and phase for the stations at Andenes, Juliusruh and Tavistock are shown in Fig. 3, 4, and 5, respectively. Every data set is compared to the NAVGEM analyzed tidal fields from a local as well as from a global perspective as already done for the mean winds and temperatures.

The observations from all stations indicate a clear winter amplitude maximum. A further maximum is evident during September. The amplitudes are smallest during November as well as during April. The latter point is not visible above Tavistock

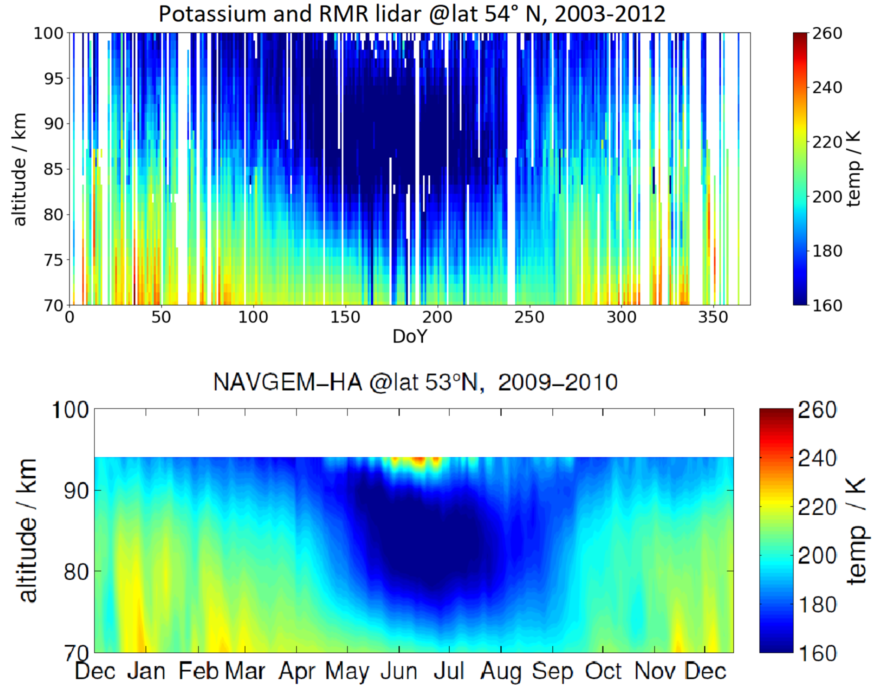

Figure 2. Comparison of mean temperatures above Kühlungsborn. The upper panel shows the temperatures derived from the potassium lidar. The lower panel shows the NAVGEM-HA ~~reanalysis~~ analysis field for the same location.

compared to the other locations. In general, the tidal amplitudes above Tavistock are also even stronger during fall than during winter. Compared to the other locations the winter maximum above Tavistock is less pronounced. In general, the amplitudes during winter are strongest for midlatitudes (Juliusruh).

The NAVGEM-HA analyzed amplitudes reveal the same temporal variability over the year as from the observations. Above an altitude of 90 km, the amplitudes from NAVGEM-HA show a significant increase which is not seen in the observations. This was also visible in the temperature data of NAVGEM-HA compared to the lidar data.

~~Next~~ In addition to the amplitudes of the semidiurnal ~~tide, also the phases over the year are calculated with the adaptive spectral filter~~tides, the annual phase bahaviour of those tides was also calculated using the spectral adaptive filter.. In general, for every location, the phase of the semidiurnal tide is slowly drifting over the year. During winter the phases are quite stable, at the beginning of March, the phase shows a sudden increase, which is evident in every location as well as in the observations and the ~~reanalysis~~ meteorological analysis data. This behavior reverses during October/November, exactly when the atmosphere is changing from summer to winter conditions and vice versa. A similar phase progression is visible from the NAVGEM-HA locally analyzed data as well as from the global fields. There is a tendency that the global fields show larger differences to the observations during summer which is due to the coarser temporal resolution of the global data.

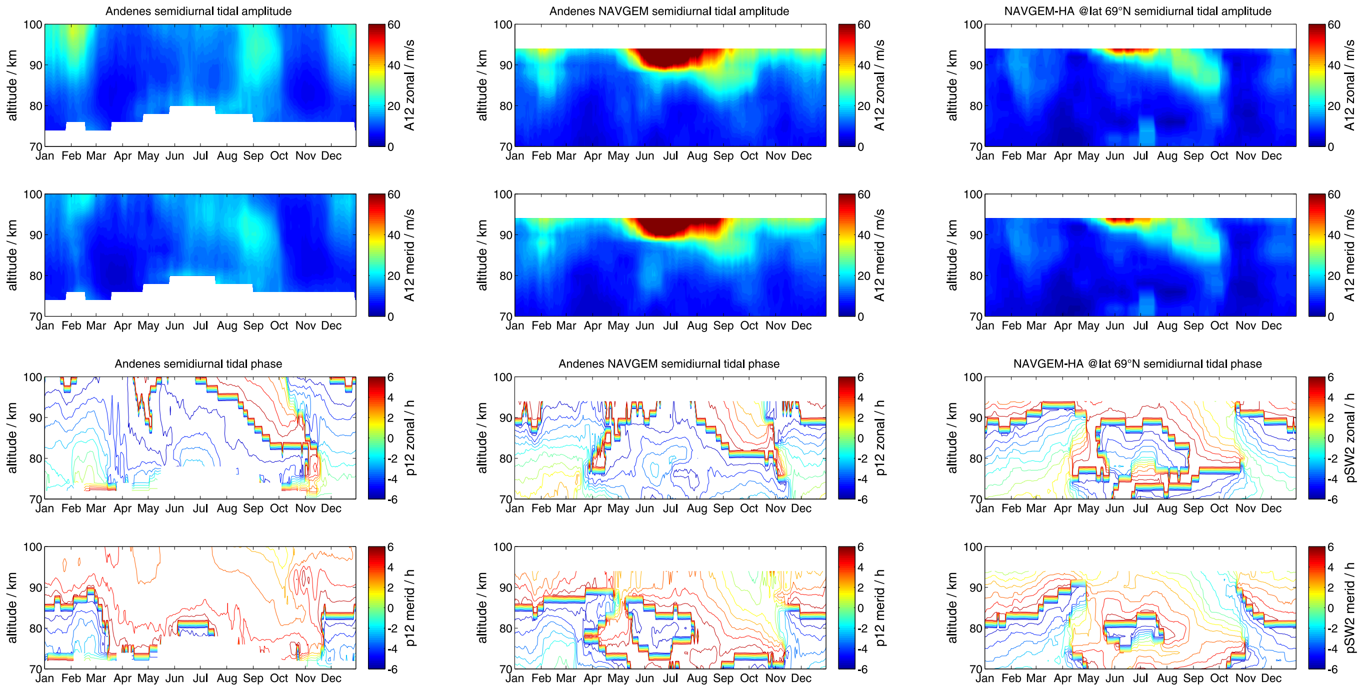

Figure 3. Comparison of semidiurnal seasonal zonal and meridional amplitude (upper two rows) and phase (lower two rows) tidal climatology using a 30-day running median with periodic boundary condition. The left panels show the meteor radar observations above Andenes (69° N, 11° E). The central panels show the NAVGEM-HA ~~reanalysis~~ analysis fields for the same period. The right panels visualize the zonal mean tidal amplitude and phase of the SW2. The label A12 and p12 corresponds to the semidiurnal amplitude and phase using the local diagnostic.

4.4 Day-to-day variability during a sudden stratospheric warming

The day-to-day variability of the mean winds, the semidiurnal tidal amplitudes and phases are investigated during the sudden stratospheric warming (SSW) in 2010 and 2013 in comparison to NAVGEM-HA analyzed data from a local perspective as well as from a global view. The analysis is done for high latitudes (Andenes) and midlatitudes (Juliusruh) in the same way.

4.4.1 Winter season 2009/2010

During the winter in 2009/2010, a major sudden stratospheric warming occurred at the end of January when the polar vortex was markedly displaced from the pole (Stober et al., 2012) and afterward showed an eventual break up into two unequal strong lobes (e.g. Dörnbrack et al., 2012; Jones Jr. et al., 2018). Following previous studies involving NAVGEM-HA the onset of the SSW occurred on 27th January (McCormack et al., 2017). Mean winds, the semidiurnal tidal amplitude and phase are shown in Fig. 6 from the meteor radar observations above Andenes as well as for the corresponding locally analyzed NAVGEM-HA data. In Fig. 7 the same results are shown for the station at midlatitudes above Juliusruh. Stronger changes in the winds are visible for Juliusruh than for Andenes. Even the semidiurnal amplitudes are stronger at midlatitudes. This is in agreement with

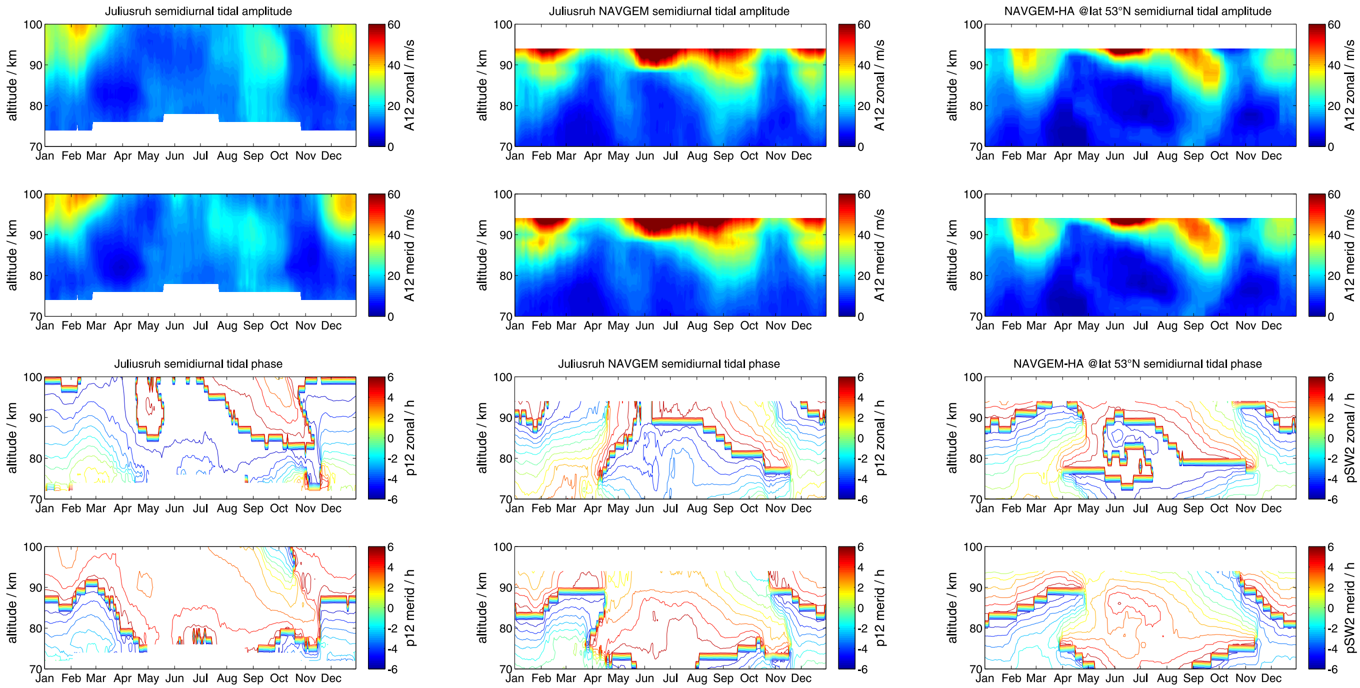

Figure 4. Comparison of semidiurnal seasonal zonal and meridional amplitude (upper two rows) and phase (lower two rows) tidal climatology using a 30-day running median with periodic boundary condition. The left panels show the meteor radar observations above Juliusruh (54.3° N, 13° E). The central panels show the NAVGEM-HA ~~reanalysis~~ analysis fields for the same period. The right panels visualize the zonal mean tidal amplitude and phase of the SW2. The label A12 and p12 corresponds to the semidiurnal amplitude and phase using the local diagnostic.

the stronger seasonal variation of the semidiurnal tidal amplitude above Juliusruh. After the onset of the sudden stratospheric warming, the semidiurnal tidal amplitudes show an enhancement at the beginning of February, which is visible at both stations and in both wind components.

The semidiurnal tidal phases show a large day-to-day variability during the winter period, which is in general stronger at high latitudes than at midlatitudes. After the central date of the sudden stratospheric warming, the tidal phase shows a sudden increase which lasts only a few days. After these days, the phase shows a ~~recovering~~ recovery where they become more stable again just as before the sudden stratospheric warming.

The NAVGEM-HA analyzed winds exhibit the same short-term variability during the 2009/2010 winter at both stations for the winds as well as for the semidiurnal tide. Even the phase enhancement after the central date of the SSW is remarkably well reflected by the NAVGEM-HA data. Some differences occur above an altitude of 85 km, where NAVGEM-HA data reveals larger magnitudes in the winds as well as larger amplitudes for the semidiurnal tide as previously seen. ~~In~~ Fig. 8 ~~the~~ shows global NAVGEM-HA results for both ~~stations from the global NAVGEM-HA shows together~~Andenes and Juliusruh station locations. The global analyzed NAVGEM-HA data exhibit much less variability during the winter compared to the locally

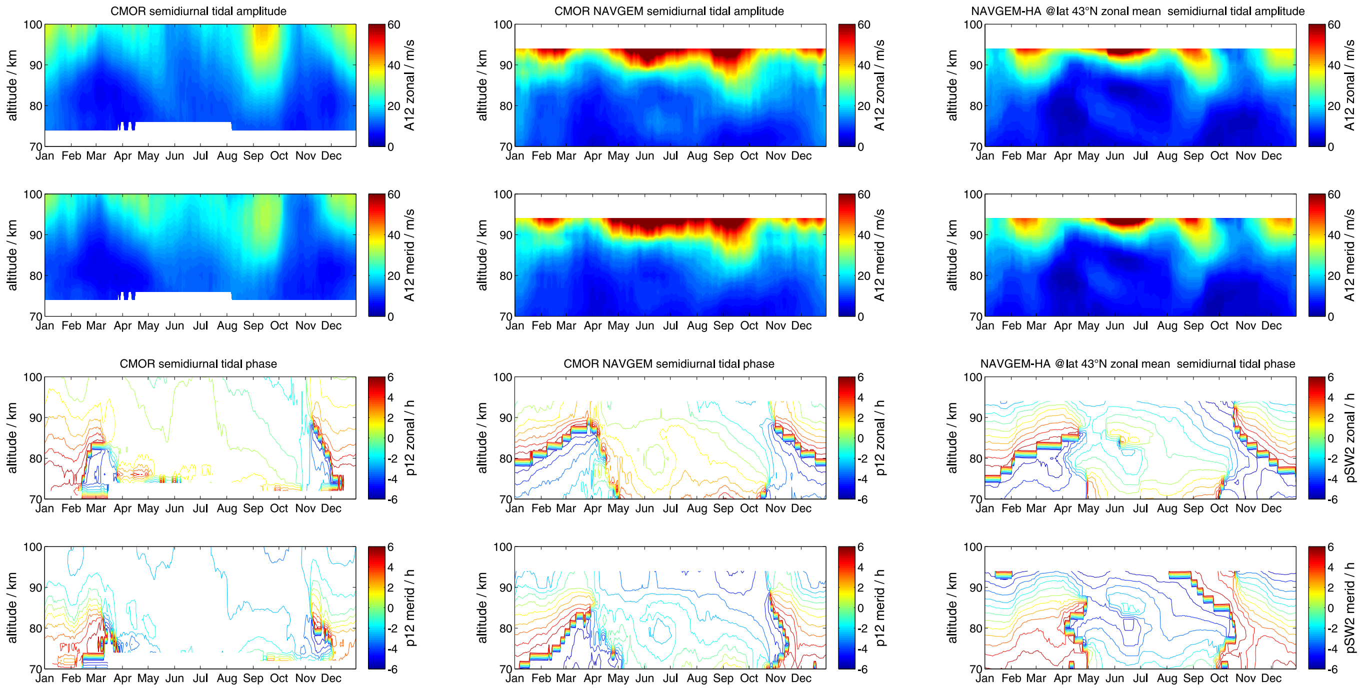

Figure 5. Comparison of semidiurnal seasonal zonal and meridional amplitude (upper two rows) and phase (lower two rows) amplitude and phase tidal climatology using a 30-day running median with periodic boundary condition. The left panels show the meteor radar observations above Tavistock (43.2° N, 80.7° W). The central panels show the NAVGEM-HA ~~reanalysis~~ analysis fields for the same period. The right panels visualize the zonal mean tidal amplitude and phase of the SW2. The label A12 and p12 corresponds to the semidiurnal amplitude and phase using the local diagnostic.

analyzed data. But the central date of the SSW is better to see in the winds than it was the case for the locally analyzed winds. However, the main features for the semidiurnal tide stay the same. The amplitudes show an increase after the central date of the SSW and the phases reveal a change for a few days at both locations. In contrast to the locally analyzed data, the phases from the global NAVGEM-HA fields slowly increase during the winter. But in general, the agreement with observations is still good.

4.4.2 Winter season 2012/2013

The winter season in 2012/2013 was also characterized by a major sudden stratospheric warming. In this case, the ~~central date of the warming was at the beginning of January 2013 and the~~ onset of the SSW occured on 7th of January using again the definition presented in McCormack et al. (2017). During the SSW the vortex was split into two lobes (Coy and Pawson, 2015). Again, mean winds, the semidiurnal tidal amplitudes and phases are shown in Fig. 9 and 10 for high latitudes and midlatitudes, respectively.

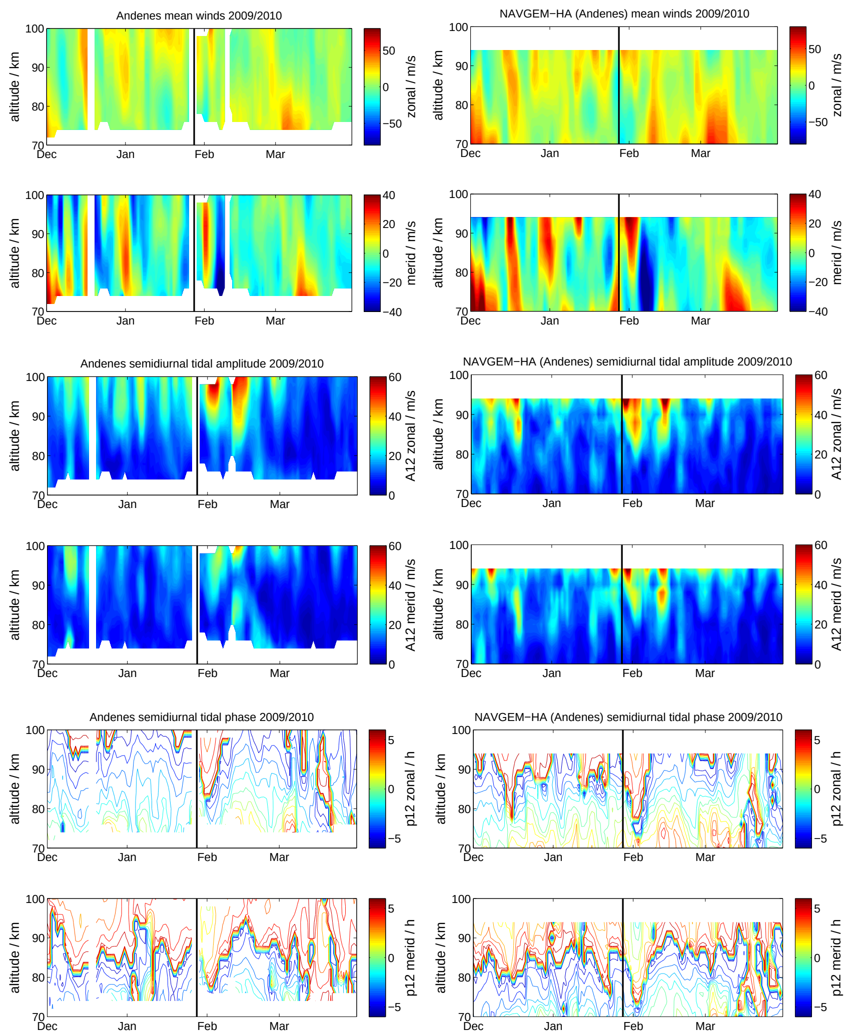

Figure 6. Comparison of meteor radar observations and NAVGEM-HA above Andenes during the winter 2009/10 for daily mean zonal and meridional winds (upper two panels), semidiurnal tidal zonal and meridional amplitude (middle panels) and semidiurnal tidal phases (lower two panels). The label A12 and p12 corresponds to the semidiurnal amplitude and phase using the local diagnostic.

In this winter season, the mean zonal winds at high latitudes are stronger, especially after the SSW, than at midlatitudes, which is opposite to that seen in the winter season 2009/2010. The mean meridional winds are similar in strength for both stations. Nevertheless, the semidiurnal tide shows again stronger amplitudes at the midlatitude station than at high latitudes. At Andenes, we see a distinct increase of the amplitudes after the SSW, which was already seen in the winter season 2009/2010,

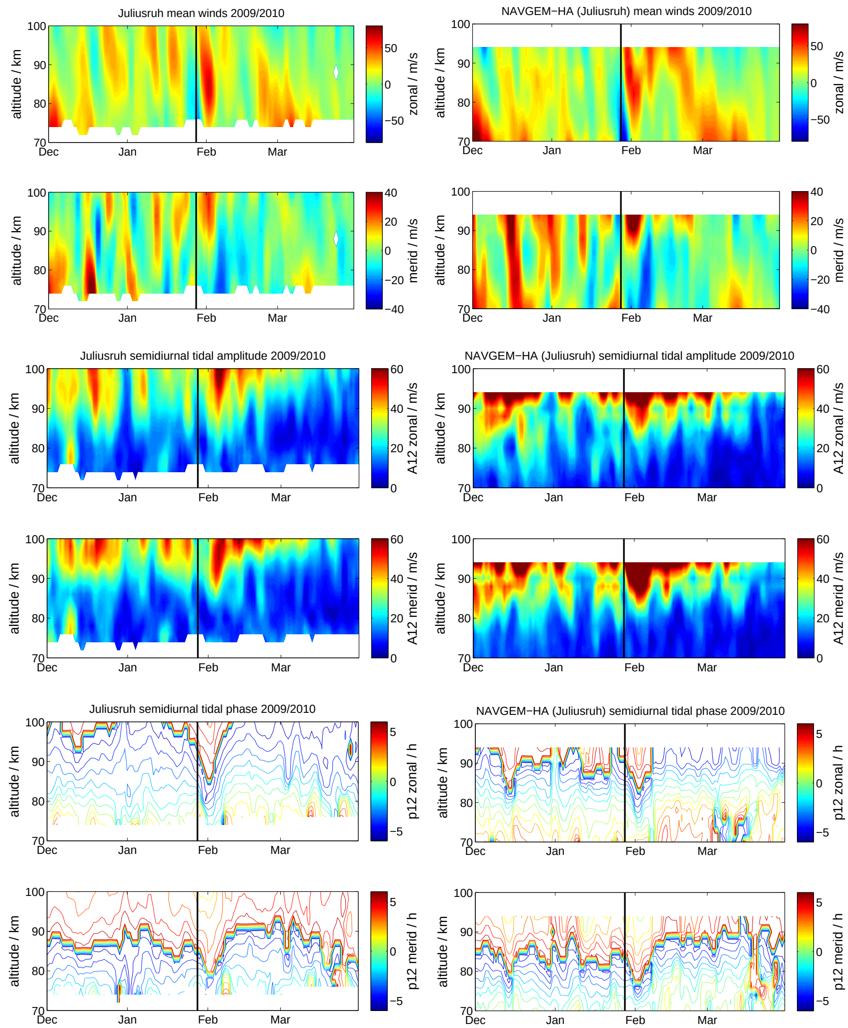

Figure 7. Comparison of meteor radar observations and NAVGEM-HA above Juliusruh during the winter 2009/10 for daily mean zonal and meridional winds (upper two panels), semidiurnal tidal zonal and meridional amplitude (middle panels) and semidiurnal tidal phases (lower two panels). The label A12 and p12 corresponds to the semidiurnal amplitude and phase using the local diagnostic.

while in general at Juliusruh a larger tidal activity is visible. Here, before and during the central date of the SSW the tidal amplitudes decrease in the first place due to the strong changing winds. Afterward, the semidiurnal tidal amplitudes increase again stronger than during the whole winter.

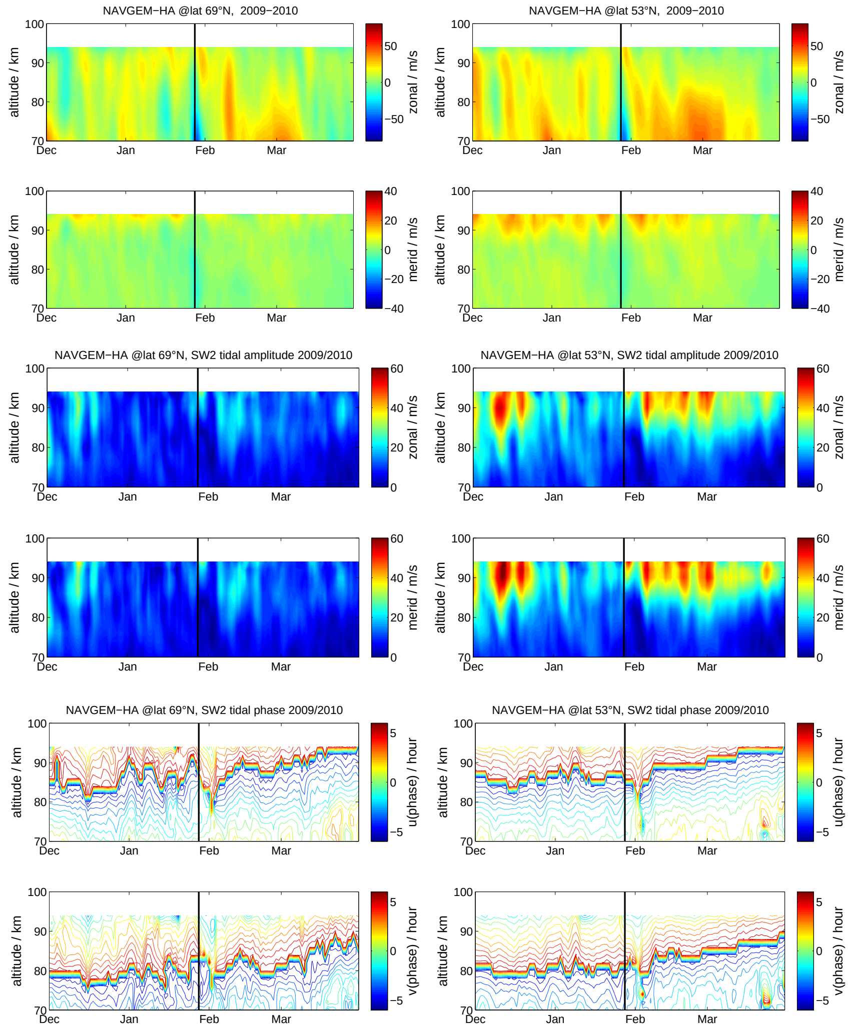

Figure 8. Comparison of global NAVGEM-HA above Andenes and Juliusruh during the winter 2009/10 for daily zonal mean zonal and meridional winds (upper two panels), zonal mean semidiurnal tidal zonal and meridional amplitude (middle panels) and zonal mean semidiurnal tidal phases (lower two panels).

The semidiurnal tidal phases show again a large variability during the whole time. A few days after the central date of the sudden stratospheric warming a sudden increase of the phase is visible in the same way as for the winter 2009/2010. The locally analyzed NAVGEM-HA data reveal structures during this winter period similar to those from the observations. Evident from every data set, the mean winds, as well as the amplitudes, are slightly overestimated in NAVGEM-HA. The NAVGEM-HA analyzed tidal phases exhibit also a sudden change after the SSW, but not as strong as from the observations, but this might be due to a general more disturbed winter period compared to the year 2009/2010. The globally analyzed data from NAVGEM-HA are shown in Fig. 11. As was the case for the 2009/2010 winter, in this winter season the winds from a global perspective are much stronger and uniformly distributed over the winter months, except for the wind reversal during the SSW, which is visible at the beginning of January.

5 Discussion

5.1 Implications of the ASF constraint by the vertical wavelength

~~Atmospheric tides are a major driver of the short term variability of the lower thermosphere/ionosphere. The developed ASF technique provides a new tool to decompose time series to assess this short term variability from local and global data sets and allows a unified data analysis from observations and models or reanalysis such as NAVGEM-HA. The benefits of the method are:~~

- ~~data can contain data gaps (gaps have to be shorter than adapted window length)~~
- ~~applicable to unevenly sampled time series~~
- ~~full error propagation through covariance matrices~~
- ~~vertical regularization for each atmospheric parameter~~

~~However~~Due to the nature of the Fourier transform and the sampling, there are ~~also~~ some drawbacks due to the short window length required to assess the short term tidal variability. The frequency bandwidth around each tidal ~~frequencies~~ frequency is rather wide. The contamination due to other waves falling into these windows, (for instance gravity waves), is minimized by the vertical regularization of the tidal vertical wavelength, which turns out to be a key element of the ASF.
The vertical regularization was implemented by allowing gradual changes with altitude for each of the derived wind components. The mean winds are regularized using a 10 km vertical retrieval kernel, the diurnal and semidiurnal tides are retrieved applying a 16 km vertical retrieval kernel. We optimized these vertical wavelength values considering the results of previous studies using meteor radars investigating the vertical wavelengths of tides (Yu et al., 2013; Davis et al., 2013; Fritts et al., 2019). These earlier studies showed that the vertical wavelengths for most of the tidal modes are much larger than >25 km. Only Yu et al. (2013) found for some Hough modes vertical wavelengths shorter than <25 km. To avoid potential contamination of shorter tidal wavelengths in our vertical retrieval kernel, we did not implement a hard cut off vertical wavelength. Instead, we just constrain the smoothness of the vertical tidal phase within the averaging kernel and even allow a gradual change.
The vertical regularization constraint is an essential feature of the ASF compared to many other diagnostic techniques based on wavelet or Fourier methods. Previous studies based on lidar observations (e.g., Ehard et al., 2015; Baumgarten et al., 2017, and reference therin) already investigated how the potential gravity wave energy changes with the applied filtering. Temporal

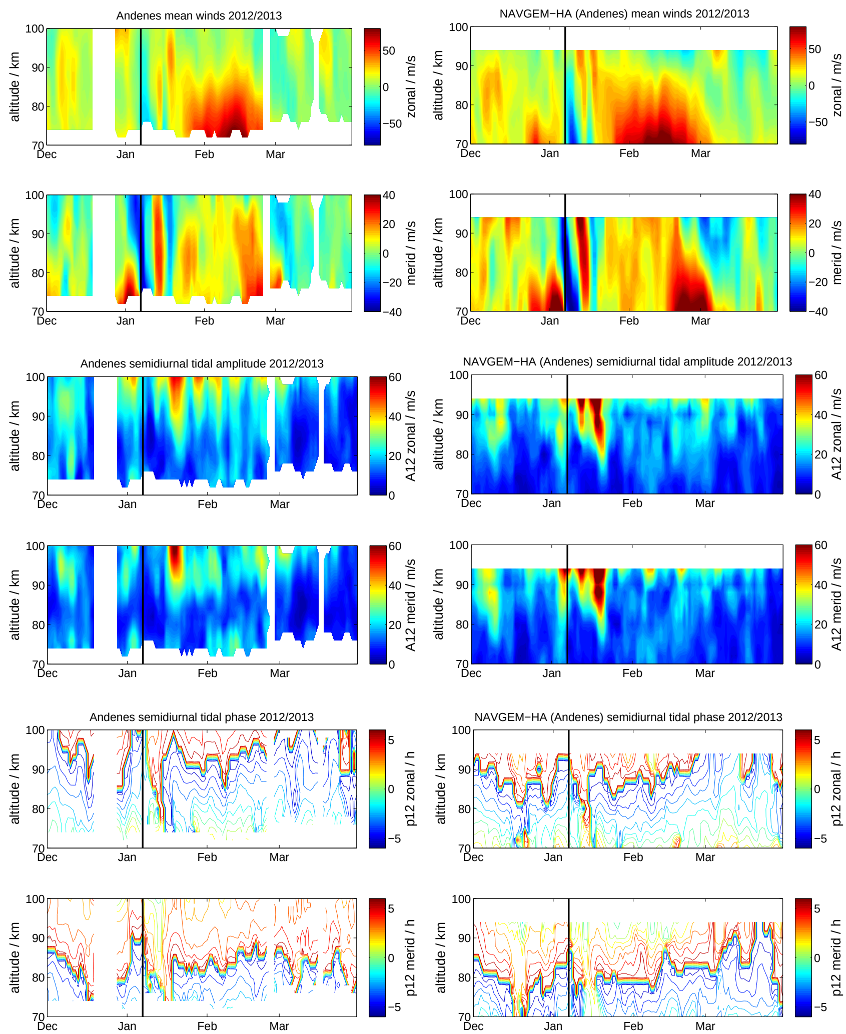

Figure 9. Comparison of meteor radar observations and NAVGEM-HA above Andenes during the winter 2012/13 for daily mean zonal and meridional winds (upper two panels), semidiurnal tidal zonal and meridional amplitude (middle panels) and semidiurnal tidal phases (lower two panels).The label A12 and p12 corresponds to the semidiurnal amplitude and phase using the local diagnostic.

filters tend to underestimate inertia gravity waves due to their long periods combined with short vertical wavelengths, whereas vertical filters are designed to eliminate the tidal contribution due to their large vertical wavelengths. As a consequence, this filter underestimates gravity waves with comparatively large vertical wavelengths. The ASF is much less prone to such biases due to the combination of spatio-temporal information for the specific waves.

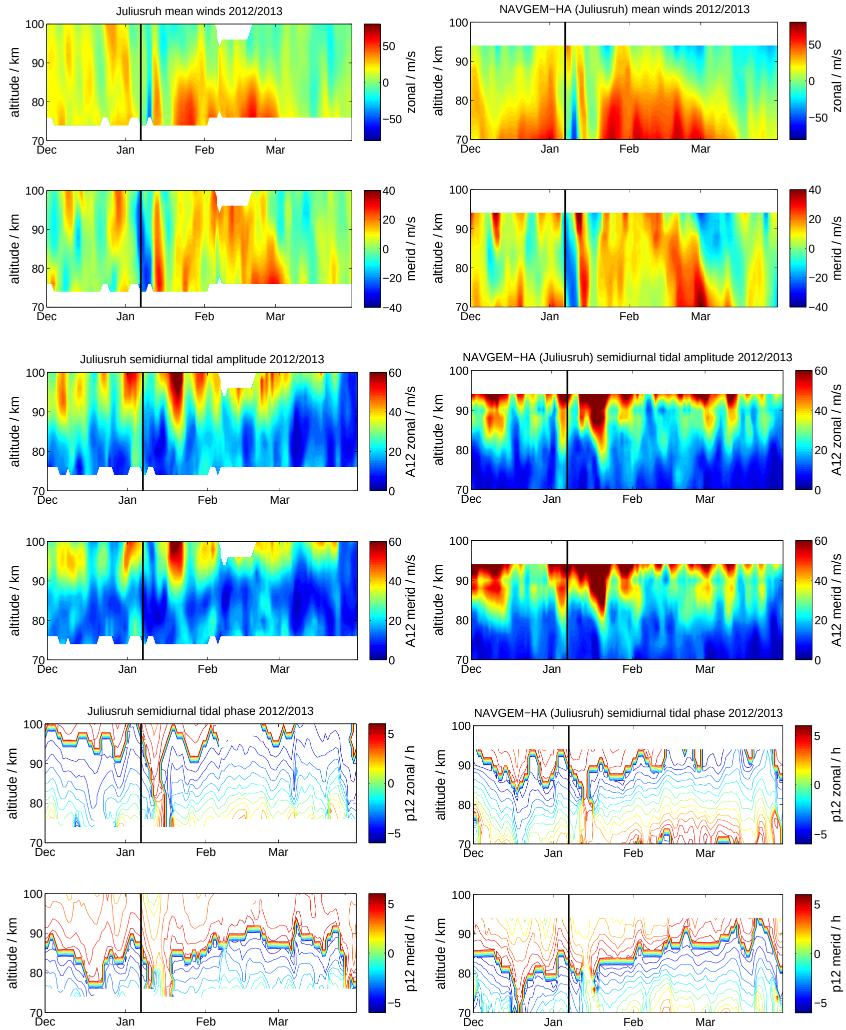

Figure 10. Comparison of meteor radar observations and NAVGEM-HA above Juliusruh during the winter 2012/13 for daily mean zonal and meridional winds (upper two panels), semidiurnal tidal zonal and meridional amplitude (middle panels) and semidiurnal tidal phases (lower two panels).The label A12 and p12 corresponds to the semidiurnal amplitude and phase using the local diagnostic.

5.2 NAVGEM-HA and MR mean wind and temperature climatology

The comparison of the NAVGEM-HA mean winds and the meteor radar climatologies at Andenes, Juliusruh and CMOR is remarkable up to an altitude of 94 km. Due to the data assimilation, NAVGEM-HA captures the main features of the seasonal

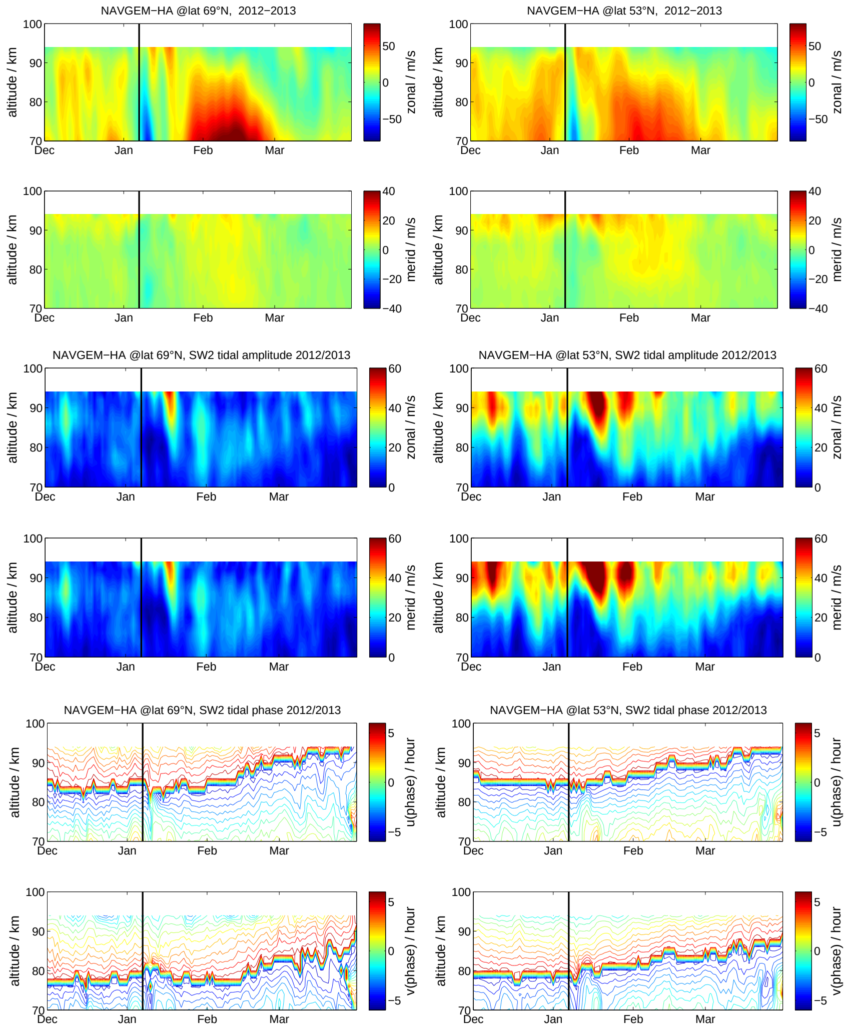

Figure 11. Comparison of global NAVGEM-HA above Juliusruh (left column) and Andenes (right column) during the winter 2012/13 for daily zonal mean zonal and meridional winds (upper two panels), zonal mean semidiurnal tidal zonal and meridional amplitude (middle panels) and zonal mean semidiurnal tidal phases (lower two panels).

wind climatologies such as the weak eastward winds during the winter, the asymmetry of the seasonal pattern between the spring and autumn wind reversals as well as the gradual descent of the summer wind reversal between the mesospheric westward winds and the higher altitude thermospheric eastward jet. The good agreement during the winter months was already outlined in McCormack et al. (2017) presenting initial cross-validation of the NAVGEM-HA winds with globally distributed and available meteor radar wind observations.

Comparing the seasonal morphology of the zonal and meridional winds between NAVGEM-HA and other comprehensive GCMs, such as WACCM or SD-WACCM ~~Smith (2012); Chandran and Collins (2014)~~(Smith, 2012; Chandran and Collins, 2014) , and the meteor radar and lidar data indicate a slightly better agreement for the meteorological ~~reanalysis~~ analysis for altitudes beyond 80 km. Similar results have been found by comparing meteor radar winds to free running mechanistic GCMs Pokhotelov et al. (2018). Smith (2012) performed a detailed assessment of the WACCM model using various ground-based and satellite measurements in the MLT and also noted some discrepancies between the observations and the model fields.

The general thermal structure and seasonal climatology are also well-reproduced in NAVGEM-HA for the lidar observations presented in Fig. 2 at the mid-latitude station of Kuehlungsborn. The ~~reanalysis~~ meteorological analysis captures the seasonal course of the altitude variation of the mesopause. Further, we identified a small offset between the lidar and the NAVGEM-HA temperatures. The ~~reanalysis~~ analysis data has a tendency toward slightly warmer temperatures compared to the resonance lidar. These slightly higher temperatures may also explain the magnitude of the mean winds from the MR observations.

At mesospheric altitudes, NAVGEM-HA assimilates satellite measurements from TIMED and AURA satellites and radiances from the Defense Meteorological Satellite program (DMSP) (Eckermann et al., 2018). Systematic differences between the meteorological ~~reanalysis~~ analysis and the data herein may have different origins. There could be intrinsic differences due to the model physics leading to such deviations or the assimilated data itself may show some systematic differences in relation to the observations used for the comparison. Further, considering that the *true* state of the atmosphere temperature and winds remains elusive, it is hard to determine which of the observational techniques provides a better representation of this *true* state. Thus, it is essential to assess some of the systematic differences, which can arise due to the methodology employed for the comparison e.g.,does applying different diagnostics or different spatio-temporal sampling of the instruments make a large difference. Validation and assessment of potential biases between the SABER temperatures and ground-based lidar measurements can be found in Xu et al. (2006); Dawkins et al. (2018). A cross comparison of the MLS and SABER temperatures is presented in Schwartz et al. (2008). A detailed description of how the data assimilation in NAVGEM-HA treats the temperature biases between both satellites is given in Eckermann et al. (2018).

Another important point ~~that requires a thorough discussion is the vertical regridding of the NAVGEM-HA datato a geometric altitude grid. NAVGEM-HA uses a fixed top level pressure of $6 \cdot 10^{-5}$ hPa (e.g., McCormack et al., 2017; Eckermann et al., 2018, and refer , which corresponds to an approximate altitude of 116 km~~ affecting the comparison is the availability of the assimilated data. ~~However, at the upper three model levels, an enhanced diffusion is applied to reduce the effects of wave reflection. These layers effectively act as a "sponge layer" and should not be included in the data analysis. McCormack et al. (2017) used for the initial validation geometric altitudes up to 95 km for the mean winds and a maximum altitude of~~ Above 90 ~~km for the wave analysis. In particular, during the cold summer months (hemispheric summer) the geometric altitude of a specific pressure level is much lower compared to the winter months. This squeezing of the pressure levels due to~~ km less satellite observations can be assimilated. Further, it has to be noted that the assimilated SABER temperatures show characteristic pattern due to the ~~much colder mesosphere explains why the agreement between the meteor radar winds and~~ yaw cycle of the spacecraft, which changes every 60 days the observing geometry providing a variable latitudinal coverage. From 52° S to 52° N the satellite collects constant measurements whereas the higher latitudes depend on the yaw cycle and alternates between up to 82° S or 82° N latitudinal coverage. This yaw cycle pattern affects the data quality of NAVGEM-HA wind components is significantly degraded beyond 90 km altitude during summer. A similar effect can be found in the temperature comparison. at Juluisruh and Andenes.

5.3 NAVGEM-HA and MR mean wind semidiurnal tidal comparison

Atmospheric tides are global-scale waves having periods which are an integer fraction of a day. At the MLT height, tides gain huge amplitudes and contribute significantly to the daily variability of the zonal and meridional winds. At mid- and polar latitudes, the semidiurnal tide is the most prominent tidal wave in the MLT that can be observed throughout the course of the year (Portnyagin et al., 2004; Pokhotelov et al., 2018; Wilhelm et al., 2019).

In principle, local observations (single measurements) can not distinguish between migrating and non-migrating tidal components and only observe a total tide. Earlier studies (e.g., Portnyagin et al., 2004) have investigated the global nature of the diurnal and semidiurnal tide at polar latitudes using a chain of radars at approximately 70° N. They found very good agreement between monthly tidal amplitudes and phases for all stations along the latitudinal circle. Recently, there have been some attempts to separate migrating and non-migrating tides using globally distributed chains of meteor radars (He et al., 2018) assuming theoretical tidal wave fields consisting of migrating and non-migrating components. However, due to the small number of meteor radars at the latitudinal circles, the analysis still contains a high degree of ambiguity.

Combining the benefits of high resolution local measurements with global meteorological reanalysis analysis data solves this problem. The comparison of the semidiurnal tidal climatology reveals that NAVGEM-HA reproduces the seasonal morphology of the tidal magnitudes for both wind components up to an altitude of 90 km applying the ASF tidal diagnostic. The local ASF diagnostic shows remarkable agreement between the global tidal analysis of the migrating SW2 tide in magnitude and phase. The non-migrating semidiurnal components show only very small and often negligible amplitudes.

5.4 NAVGEM-HA and MR winds and tidal day-to-day variability and lunar tides during SSW events

In this study, we present a cross-comparison of mean winds and semidiurnal tidal day-to-day variability during two SSW events. Such short time variations are essential for the understanding of the forcing from below of the thermosphere and ionosphere (Liu, 2016). Meteorological reanalysis data, such as NAVGEM-HA, provide a much more realistic forcing of the upper atmosphere due to tides and mean winds compared to current versions of other comprehensive models. Chandran and Collins (2014) investigated SSW events using WACCM-SD nudged with reanalysis fields from the GEOS-5.2 reanalysis system up to an altitude of about 40 km. However, at altitudes above 70-80 km the nudged model started to substantially deviate from the observed wind climatologies (Wilhelm et al., 2019). In particular, the nudged model showed a wind reversal from eastward to westwards winds between 70-80 km, which is not confirmed from the wind climatologies. Such reversal of the zonal wind can be also found in other comprehensive models or mechanistic models (Smith, 2012; Becker, 2012). Liu (2016) shows a comparison among several GCMs indicating that there are substantial deviations at the mesosphere and upper atmosphere,

~~although each of the GCMs was nudged up to the lower stratosphere (see also Pedatella et al. (2014) for more details). Only the GAIA model (Jin et al., 2012; Liu et al., 2014) showed during winter eastward winds at the MLT.~~ Besides comparing mean winds, we also investigated the day-to-day variability of the semidiurnal tide during two winter seasons with a major SSW event at the mid-latitude location Juliusruh and polar latitudes above Andenes. ~~Atmospheric tides are generated in the troposphere and stratosphere mostly through the absorption of sunlight by water vapor and ozone (e.g., Lindzen, 1979).~~ In 2010 there was a vortex displacement event (e.g., Stober et al., 2012; Matthias et al., 2013), which was already validated by a cross comparison of the mean winds and waves in McCormack et al. (2017) using several worldwide-distributed meteor radars. The second SSW event occurred during winter 2012/13 and evolved as a vortex splitting event (e.g., Xu and San Liang, 2017).

Daily mean winds and tidal amplitudes were diagnosed by the ASF. The meteorological ~~reanalysis~~ analysis of NAVGEM-HA reproduces the general day-to-day variability of winds and even shows a high level of agreement for individual planetary waves passing over the stations. In particular, the timing of the SSW event itself with the zonal wind reversal and the formation of an elevated stratopause is well-captured. Similar to the zonal and meridional wind climatologies, the ~~reanalysis~~ meteorological analysis tends to show higher magnitudes of the winds. Previous comparison of wind observations to ~~reanalysis~~ model data, such as ECMWF or MERRA2, were limited to a maximum altitude of approximately 70-75 km and below (Rüfenacht et al., 2018) and, thus, we omit here any further detailed discussion.

Another very important aspect of this study is the phase variability on a day-to-day basis. The ASF provides information on the phase stability of tides with basically the same resolution as the original measurement time series. Very often tidal phases are assumed to be stable over long periods of up to several months in the analysis. However, for instance, the TIMED satellite requires 60-days to cover all local times due to its orbit geometry (Zhang et al., 2006; Oberheide et al., 2011). Our results indicate that during an SSW the phase of the SW2 tide is significantly altered on a global scale as well as on a regional or local scale as the dynamics of the middle atmosphere change (e.g., Manney et al., 2009; Matthias et al., 2012). Fuller-Rowell et al. (2016) discussed three possible mechanisms to understand these changes of the tide; Fuller-Rowell et al. (2010); Jin et al. (2012) attributed the change of the migrating tidal phase to changes of the mean winds in the middle atmosphere, whereas Pedatella and Forbes (2010) suggested non-migrating tides as a source of the SW2 phase variability. Other studies favor an amplification of the lunar tide during an SSW (Fejer et al., 2010; Forbes and Zhang, 2012).

We want to disentangle these three aspects using the results obtained from the ASF decomposition of the local and global measurements and meteorological ~~reanalysis~~ analysis data. Fejer et al. (2010) investigated vertical plasma drifts above ~~Jicarmarca~~ Jicamarca and found a drift in local time of the semidiurnal oscillation, which was attributed to the lunar tide assuming that all other tidal waves remained stationary and monochromatic. Later Forbes and Zhang (2012) proposed that the lunar tide enhancement is a result of a shifting of the ~~Perkeris resonance~~ semidiurnal tide towards the Pekeris resonance and, hence, to the lunar tide M2 (12.42 h) due to changes in the mean zonal winds caused by the SSW. They tested the proposed physical mechanism on satellite observations from SABER, CHAMP and GRACE and the steady state Global-Scale-Wave-Model (GSWM). To separate the lunar tide from the semidiurnal SW2 tide, they used a window of 24 days to ensure sufficient frequency resolution and assumed monochromatic and stationary tidal waves within the window.

However, our analysis of the day-to-day variability indicates that the tidal phase are not stable with time and show significant variability, which appears to be related to changes in the zonal wind in the middle atmosphere driven by the polar vortex and planetary waves. Considering that a time dependent phase corresponds to a frequency shift, it is possible to convert this temporal variability into a frequency shift and, hence, estimate the spectral line shape of the tide or to derive a holographic representation of the temporal evolution on a day to day basis.

The hologram is derived considering that the tide can be represented by a cosine wave with amplitude A (e.g. semidiurnal tide), a mean frequency w and a time dependent phase $\phi(t)$;

$$A(t) = A\cos(wt + \phi(t)) \ . \tag{3}$$

Although the true functional form of the time dependent phase might be unknown, we can express this function as a Taylor series at a certain point in time t;

$$\phi(t) = \phi_0 + \frac{d\phi}{dt} \cdot t + \ldots. \tag{4}$$

Truncating the Taylor series at the first order and inserting them in eq. 3 leads to;

$$A(t) = A\cos(wt + \phi_0 + \frac{d\phi}{dt} \cdot t) \ . \tag{5}$$

Rearranging the terms according to their time dependence leads to;

$$A(t) = A\cos((w + \frac{d\phi}{dt}) \cdot t + \phi_0) \ . \tag{6}$$

It is now straight forward to numerically obtain the time dependent phase change $d\phi/dt$ using a central differences approach in the complex domain.

In Fig. 12 we show a holographic reconstruction based on the ASF decomposition of the semidiurnal tide. This technique only assumes monochromaticity within the adopted window length (less than a day for the semidiurnal tide) and, thus, captures non-stationary processes on an interday basis. The hologram shows that during the SSW event in 2012/13 the phase behavior of the semidiurnal tide itself is shifted to the period range that is expected for the lunar tide M2 (solid white line) and N2 (dashed white line). ~~Moreoverr,~~ The hologram for the global diagnostic is shown in Fig. 13. The main differences in the holograms between the local MR observations and the global tidal fields from NAVGEM-HA are attributed to the decomposition of the global fields into migrating and non-migrating tides. As shown in the appendix B there is an excitation of the non-migrating tides SW1 and SW3, which leads to the differences in the holographic reconstruction. The local diagnostic shows the superposition of all tidal components. However, the global diagnostic also indicates the frequency shifts of the SW2 tide to periods that can match the predicted Pekeris lunar tide resonances. The effect of the SSW is visible in both holograms up to 10 days after the onset of the SSW, which is also the time delay corresponding to the amplification of the semidiurnal tide after the SSW.

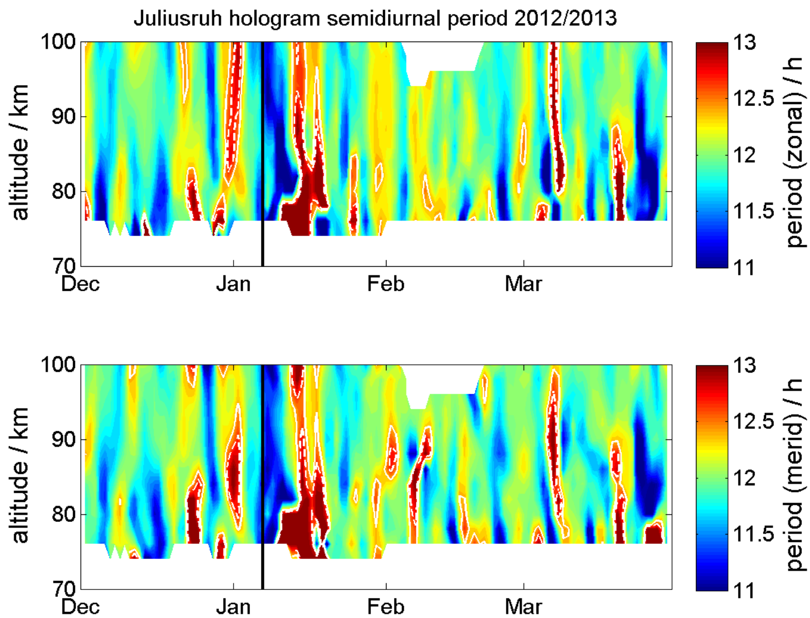

Figure 12. Holographic reconstruction of the semidiurnal tidal phase variability. The hologram shows the periods using a time variable phase, which is equivalent to a frequency shift or change in period. The white contour lines indicate the lunar tide M2 (12.42 h) (solid line) and N2 (12.66 h) (dashed line).

Moreover, Forbes and Zhang (2012) reported a delay of 5 days between the occurrence of the lunar tide amplification and the central day of the SSW event. This delay of approx. 5 days is consistent with the holographic analysis, which also shows that the frequency/period shift towards the lunar tide frequency/period (M2 and N2) occurs after the SSW event, at the beginning of the formation of an elevated stratopause or when the polar vortex begins to restore.

Many publications investigating lunar tides use window lengths that are long enough to ensure an unambiguous frequency resolution to separate the lunar tide from the semidiurnal tide, which requires at least 21-days or more ~~(e.g., Forbes and Zhang, 2012; Conte et al~~ (e.g., Forbes and Zhang, 2012; Chau et al., 2015; Conte et al., 2017; He et al., 2018; Siddiqui et al., 2018, and reference therein) . The ASF analysis indicates that there is a considerable interday tidal variability in amplitude and phase, which poses a challenge to the signal processing. Such intermittent behavior suggests that long windows (longer than even a day) might lead to spurious results, and do not allow separation of the different waves from each other. ~~SSWs~~ The zonal wind reversal and cooling at the MLT during a SSW last only for a few days (much shorter than the typical window length used for the lunar tides) and cause significant changes in zonal mean wind at mid- and polar latitudes altering the propagation conditions for the tides. As a consequence, such a long window would not allow one to capture SSW effects, which themselves cause changes in the semidiurnal tide. Thus, if one does not notice that an SSW occurred, one cannot know whether the ~~12.4 hour~~ 12.42 h tide is lunar or a semidiurnal tide that was altered by the SSW.

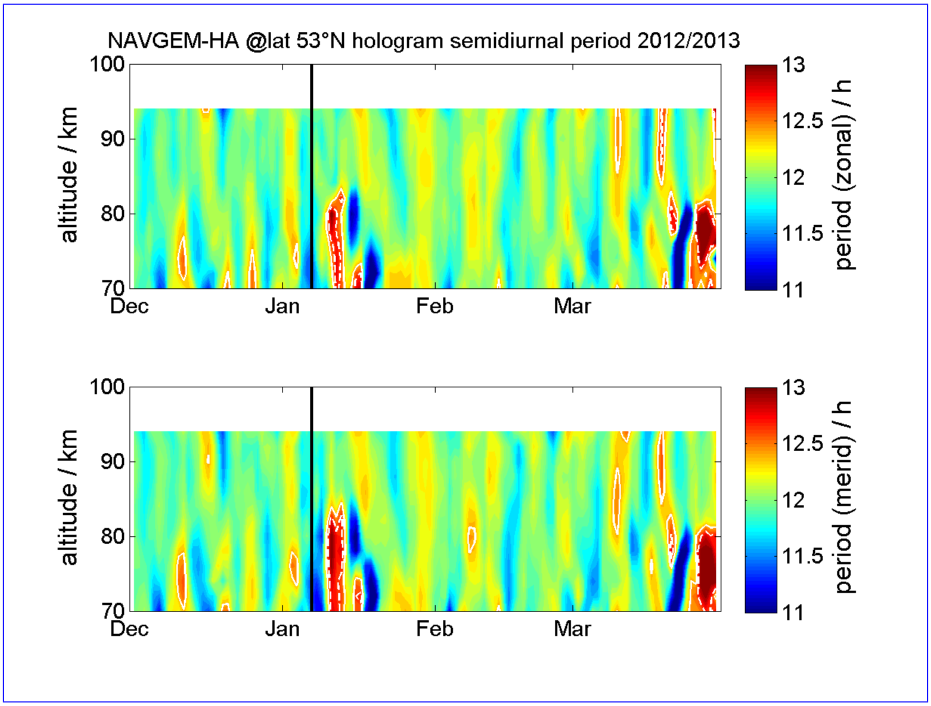

Figure 13. Holographic reconstruction of the SW2 tidal phase variability from the global diagnostic of NAVGEM-HA. The hologram shows the periods using a time variable phase, which is equivalent to a frequency shift or change in period. The white contour lines indicate the lunar tide M2 (12.42 h) (solid line) and N2 (12.66 h) (dashed line).

We also investigated the non-migrating tidal components (see appendix B) from the NAVGEM-HA. It appears that only the SW1 and SW3 tides show a response to the SSW event depending on the latitude and how the SSW evolved. This is consistent with previous studies (Liu et al., 2010). The SW3, SE1, SE2, SE3 and S0 semidiurnal tides show much smaller amplitudes and are negligible compared to the SW2 tide, in particular, at polar latitudes. Another interesting aspect when comparing the migrating and non-migrating tides from NAVGEM-HA is the winter seasonal phase behavior of the SW2 tide. The phase of the tide drifts by several hours between December to March, which correlates to the mean wind morphology. Apparently, the change of the phase of the semidiurnal tide is not explainable by a superposition of migrating and non-migrating tides. However, this needs to be examined in more detail and is beyond the scope of this paper.

Based on the present analysis, there was no amplification of the lunar tide at mid- and high-latitudes during the two examined SSW events. Previous analysis of the lunar tide facilitating multi-year observations from meteor radars by Sandford et al. (2006) showed that the signal is much weaker compared to the total S2 tide. Their spectral analysis also confirms that tides show some spectral broadening. Such a line broadening is also found in our holographic analysis. ~~In~~

Fig.14 shows the histograms of the frequency distributions obtained from the holograms. The left two panels are computed from the meteor radar observations at Juliusruh (zonal and meridional) and the right two panels from the global diagnostic using NAVGEM-HA at the same latitude (zonal and meridional, respectively). The spectral line shape seems to agree from

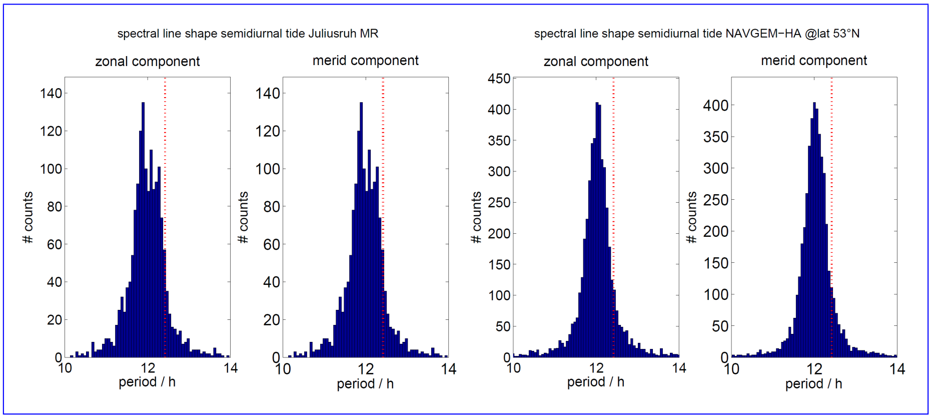

Figure 14. Histograms for the zonal and meridional frequency shift due to a temporal variable phase derived from the holograms. The left two panels show the local meteor radar observations at Juliusruh and the right two panels the global diagnostic inferred from NAVGEM-HA.

their general morphology, in particular, the line width. The vertical dashed line denotes the period of the Pekeris resonance, which lies in the natural line width of the SW2 tide. However, the peak of the spectral line obtained from the meteor radar observations at Juliusruh shows two side peaks that can be associated to the vortex splitting event and are related to the planetary wave activity during the winter 2012/13. During the vortex displacement event in the winter season 2009/10 the spectral line at Juliusruh is entirely symmetric similar to the global diagnostic for both cases. The global diagnostic is not prone to this type of effect as all longitudes are included in the analysis and, hence, these particularities average out. In the case of lunar tide amplification the global diagnostic should reveal a shoulder at the Pekeris resonance or asymmetry around the dashed vertical line, which is seems to be not present. In principle, it is possible to separate the lunar tide from the semidiurnal tide by modeling the line shape of the S2 tide.

Similar to previous studies (Fuller-Rowell et al., 2010, 2016) we attribute the day-to-day variability of the semidiurnal tidal amplitudes and phases to changes of the zonal winds in the middle atmosphere altering the vertical propagation conditions. Although atmospheric tides are global scale waves, their vertical propagation depends on the regional meteorological situation. As a consequence, the observed period or phase at the MLT can be altered. Due to the long horizontal wavelength of the semidiurnal tide, a change in the wind pattern in the middle atmosphere manifests as changes in phase for a single station measurement accompanied by a change of the vertical wavelength of the tide. The holographic reconstruction shows that the day-to-day variability of phase is equivalent to a Doppler shifting of the intrinsic tidal frequency, which causes the line broadening at the MLT.

6 Conclusions

In this study, we cross-validate the meteorological reanalysis analysis model NAVGEM-HA with ground-based meteor radar and lidar observations at mid- and high latitudes. For the validation, we performed a detailed analysis of mean winds and temperatures and atmospheric tides using a recently developed tool called adaptive spectral filter (ASF). We present a climatological comparison of mean winds, temperatures and the semidiurnal wind tide and its phase behavior. We also presented a detailed discussion of the day-to-day variability of the semidiurnal tide during two SSW events in 2009/10 and 2012/13 combining global and local diagnostics. We discussed our results in the context of previous studies, in particular, on the lunar tide amplification during SSWs and have outlined potential issues due to the day-to-day semidiurnal tidal variability. Our main conclusions are:

- The agreement between MR/lidar climatologies and NAVGEM-HA reanalysis analysis data is remarkably good compared to the seasonal wind and temperature pattern of comprehensive models. NAVGEM-HA tends to show slightly higher winds and temperatures compared to the ground-based instruments.

- NAVGEM-HA reflects the day-to-day variability of the wind and semidiurnal tide amplitude and phase behavior during SSW events.

- The temperature and wind fields in NAVGEM-HA are realistic compared to ground-based sensors up to an altitude of 90 km (geometric altitude).

- NAVGEM-HA reflects the day-to-day variability of the wind and semidiurnal tide amplitude and phase behavior during SSW events.

- The combination of NAVGEM-HA meteorological reanalysis analysis data and ground-based observations allowed us to develop new diagnostics to retrieve atmospheric information and to investigate physical processes. The cross-validation suggests that the global fields of NAVGEM-HA can be used to provide a realistic nudging for other GCMs coupling the middle atmosphere to the upper atmosphere. In particular, the good agreement of the tidal phases provides an essential quality benchmark for the lower forcing of the thermosphere and ionosphere through atmospheric tides.

- The ASF diagnostic allows us to capture the intermittent tidal behavior on a day-to-day basis and is applicable to different data sets.

- The semidiurnal tidal phase shows a significant variation over the year. This is highly relevant for the extraction of tides from satellite measurements or for the determination of the lunar M2 tide.

- The ASF and holographic analysis provides no signature of a lunar tide amplification during SSW events at mid- and high latitudes as reported by Forbes and Zhang (2012); Conte et al. (2017); He et al. (2018). However, we confirmed that the SSW event causes a shift of the semidiurnal tide towards the Perkeris Pekeris resonance, which occurs 3-5 days after the SSW.

– The day-to-day tidal variability (amplitude and phase) of the semidiurnal tide is attributed to changes in the wind pattern in the middle atmosphere altering the vertical propagation conditions of the tide. This is in agreement with previous studies by Fuller-Rowell et al. (2010); Jin et al. (2012); Fuller-Rowell et al. (2016).

In this work we demonstrate the value of meteorological reanalysis analysis data from NAVGEM-HA to investigate the day-to-day variability of tides in a global context and for local meteor radar observations. Such data sets are essential for nudging thermospheric and ionospheric models for space weather applications. Further, we emphasized that new analysis techniques are required to infer the tidal variability or to separate lunar tides from the semidiurnal tide. Holographic reconstructions and spectral line models for atmospheric tides might be part of such a solution.

Data availability. The meteor radar can be obtained from Gunter Stober upon request from the Leibniz-Institute for Atmospheric Physics. The NAVGEM-HA data used in this study can be obtained from (https://map.nrl.navy.mil/map/pub/nrl/navgem/iap). The lidar observations are available upon request from Kathrin Baumgarten.

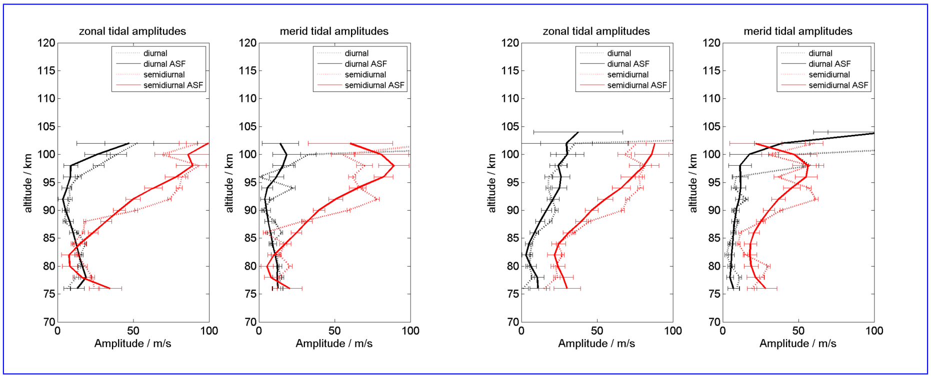

Figure A1. Here we show observations from 1st February 2010 and the Juliusruh meteor radar. The dashed lines indicate the tidal solution applying only temporal fitting and solid line shows the ASF solution with vertical regularization for the diurnal and semidiurnal tide.

Appendix A: Comparison of ASF with and without vertical regularization

Here we provide two examples comparing a tidal amplitude fit for the zonal and meridional component using the 1D ASF and the 2D ASF with vertical regularization to demonstrate how a potential contamination of gravity waves with short vertical wavelengths is reduced. The time difference between the left two panels and the right two panels is 6 hours.

Appendix B: Tidal components from global NAVGEM-HA analyzed winds

In addition to the semidiurnal tide locally observed from the meteor radar as well as from NAVGEM analyzed winds here we provide the results for the westward- and eastward-propagating non-migrating semidiurnal tidal components (SW1, SW3, SE1, SE2, SE3) as well as for the stationary semidiurnal tide (S0) during the winter 2009/2010 and 2012/2013 for the stations at Andenes and Juliusruh from the global fields of NAVGEM-HA.

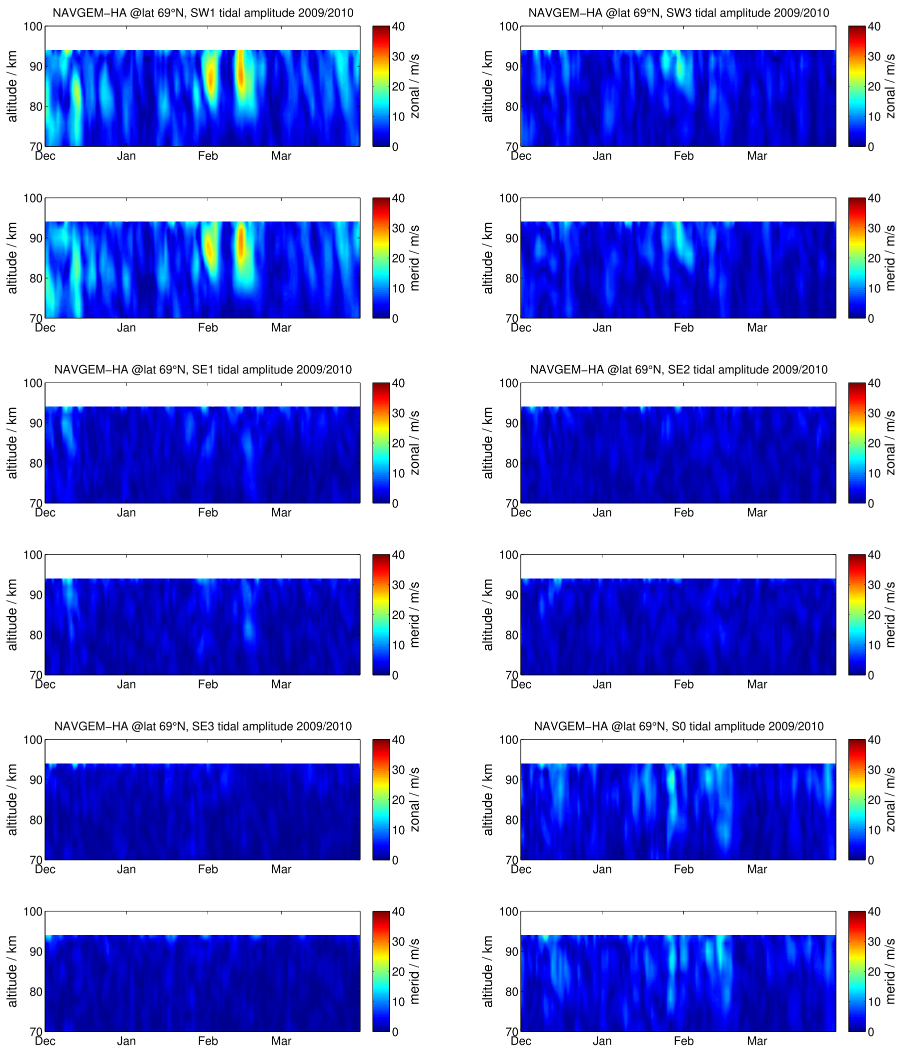

Figure B1. Non-migrating tides derived from global NAVGEM-HA winds above Andenes during the winter 2009/10 for SW1 and SW3 (upper two panels), SE1 and SE2 (middle panels), and SE3 and S0 (lower two panels) tidal components.

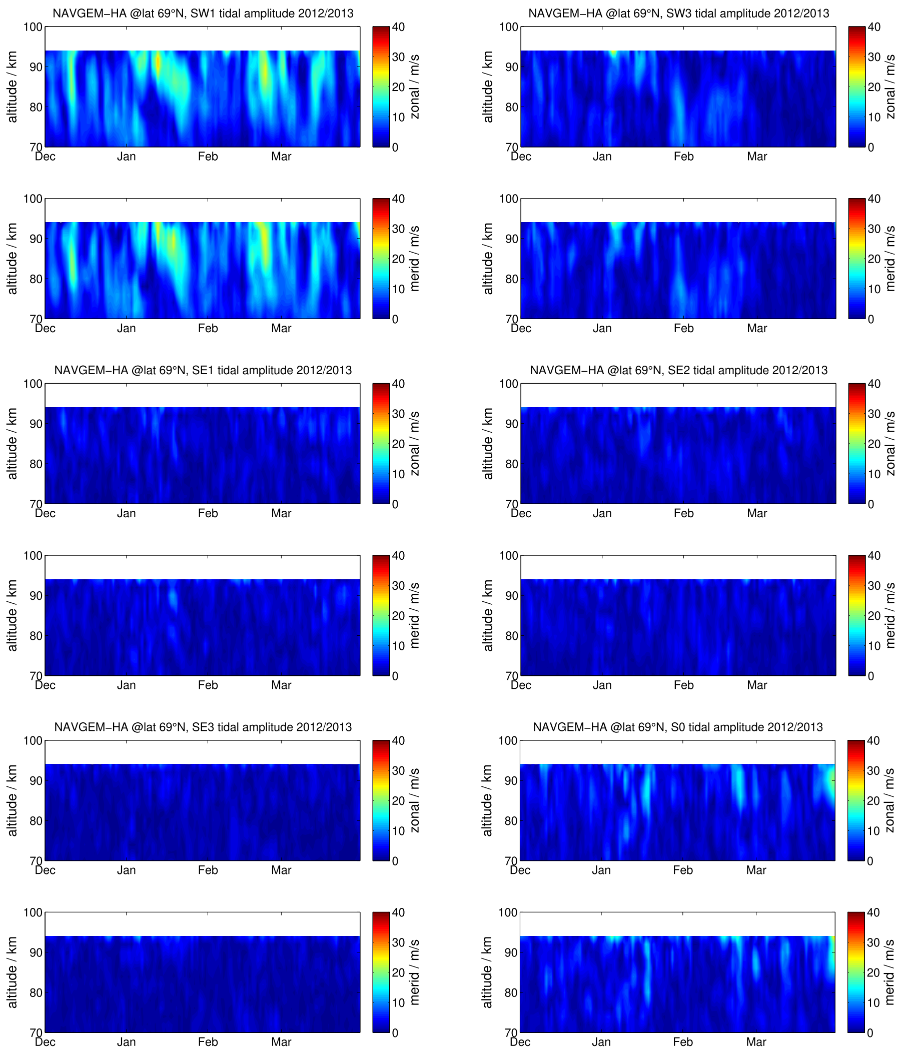

Figure B2. The same as Fig. 13 but for the winter 2012/2013.

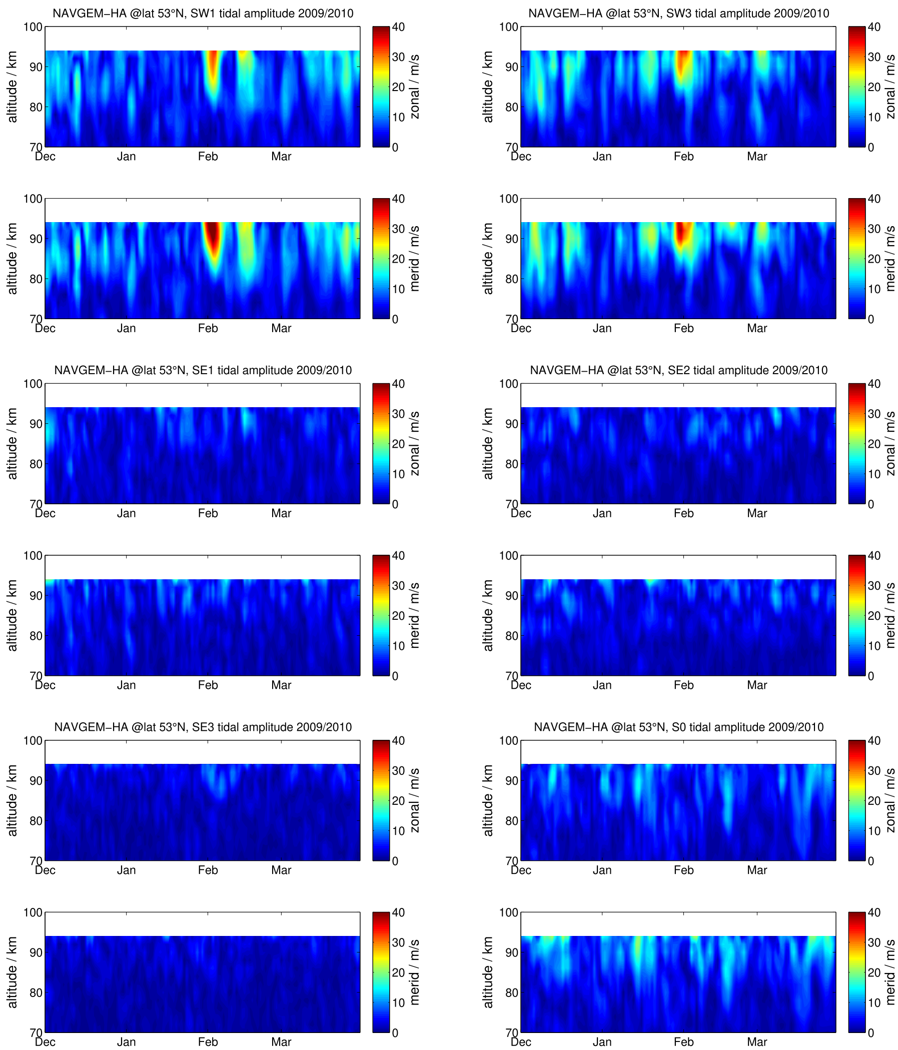

Figure B3. The same as Fig. 13 but above Juliusruh and for the winter 2009/2010.

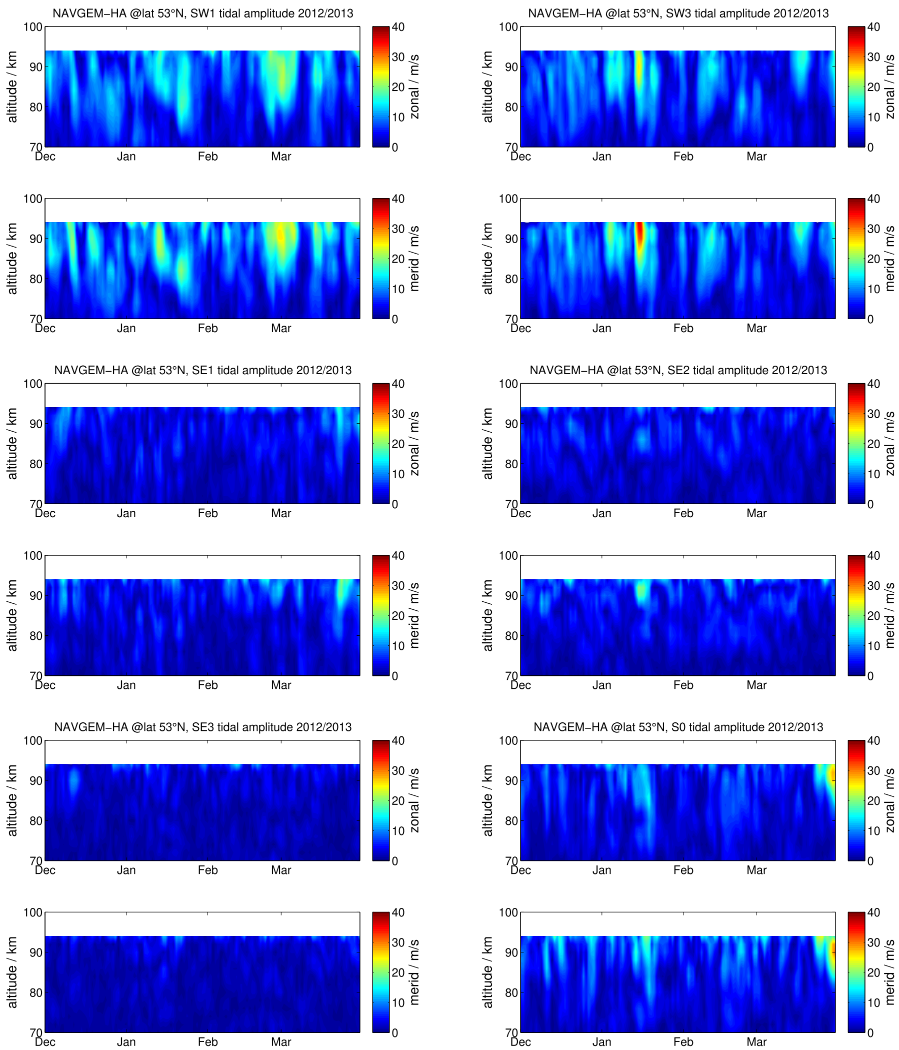

Figure B4. The same as Fig. 13 but above Juliusruh and for the winter 2012/2013.

Author contributions. The manuscript is edited and discussed with all authors. The conceptual idea of the manuscript was developed by Gunter Stober, Kathrin Baumgarten and John McCormack. The meteor radar data analysis is performed by Gunter Stober. Kathrin Baumgarten computed partly the lidar temperatures and analyzed both lidar data sets. Peter Brown contributed with the CMOR radar data, read and edited the manuscript and helped with the discussions. Jerry Czarnecki provided support in the data analysis and helped discussing the results.

Acknowledgements. This work is supported by the University of Bern Institute of Applied Physics and the Oeschger Center for Climate Change Research. Kathrin Baumgarten is supported by the Deutsche Forschungsgemeinschaft (DFG; German Research Foundation) under project LU1174/8-1 (PACOG) of the research unit FOR1898 within the Research Unit MS-GWaves. The work at the Naval Research Laboratory was supported by the Chief of Naval research and by a grant of computer time from the High Performance Computing Modernization Program. We gratefully acknowledge Michael Gerding, Michael Priester and Torsten Köpnick for the maintenance and operation of the lidar systems at IAP as well as all students for helping in lidar operation. We appreciate the support from Josef Höffner in computing the resonance lidar temperatures. We acknowledge the technical support of the IAP technicians in the operation of the meteor radars.

References

Akmaev, R. A.: WHOLE ATMOSPHERE MODELING: CONNECTING TERRESTRIAL AND SPACE WEATHER, Reviews of Geophysics, 49, https://doi.org/10.1029/2011RG000364, https://agupubs.onlinelibrary.wiley.com/doi/abs/10.1029/2011RG000364, 2011.

Alpers, M., Eixmann, R., Fricke-Begemann, C., Gerding, M., and Höffner, J.: Temperature lidar measurements from 1 to 105 km altitude using resonance, Rayleigh, and rotational Raman scattering, Atmos. Chem. Phys., 4, 793–800, 2004.

Andrews, D., Holton, J., and Leovy, C.: Middle Atmosphere Dynamics, International Geophysics, Elsevier Science, https://books.google.de/books?id=N1oNurYZefAC, 1987.

Baumgarten, K. and Stober, G.: On the evaluation of the phase relation between temperature and wind tides based on ground-based measurements and reanalysis data in the middle atmosphere, Annales Geophysicae, 37, 581–602, https://doi.org/10.5194/angeo-37-581-2019, https://www.ann-geophys.net/37/581/2019/, 2019.

Baumgarten, K., Gerding, M., and Lübken, F.-J.: Seasonal variation of gravity wave parameters using different filter methods with daylight lidar measurements at midlatitudes, Journal of Geophysical Research: Atmospheres, 122, 2683–2695, https://doi.org/10.1002/2016JD025916, https://agupubs.onlinelibrary.wiley.com/doi/abs/10.1002/2016JD025916, 2017.

Baumgarten, K., Gerding, M., Baumgarten, G., and Lübken, F.-J.: Temporal variability of tidal and gravity waves during a record long 10-day continuous lidar sounding, Atmospheric Chemistry and Physics, 18, 371–384, https://doi.org/10.5194/acp-18-371-2018, https://www.atmos-chem-phys.net/18/371/2018/, 2018.

Becker, E.: Dynamical Control of the Middle Atmosphere, Space Science Reviews, 168, 283–314, https://doi.org/10.1007/s11214-011-9841-5, http://dx.doi.org/10.1007/s11214-011-9841-5, 2012.

Becker, E.: Mean-Flow Effects of Thermal Tides in the Mesosphere and Lower Thermosphere, Journal of the Atmospheric Sciences, 74, 2043–2063, https://doi.org/10.1175/JAS-D-16-0194.1, https://doi.org/10.1175/JAS-D-16-0194.1, 2017.

Brown, P., Weryk, R., Wong, D., and Jones, J.: A meteoroid stream survey using the Canadian Meteor Orbit Radar: I. Methodology and radiant catalogue, Icarus, 195, 317–339, https://doi.org/https://doi.org/10.1016/j.icarus.2007.12.002, http://www.sciencedirect.com/science/article/pii/S0019103507005994, 2008.

Chandran, A. and Collins, R. L.: Stratospheric sudden warming effects on winds and temperature in the middle atmosphere at middle and low latitudes: a study using WACCM, Annales Geophysicae, 32, 859–874, https://doi.org/10.5194/angeo-32-859-2014, https://www.ann-geophys.net/32/859/2014/, 2014.

Chandran, A., Collins, R., and Harvey, V.: Stratosphere-mesosphere coupling during stratospheric sudden warming events, Advances in Space Research, 53, 1265–1289, https://doi.org/https://doi.org/10.1016/j.asr.2014.02.005, http://www.sciencedirect.com/science/article/pii/S0273117714000933, 2014.

Chapman, S. and Lindzen, R.: Atmospheric Tides: Thermal and Gravitational, Gordon and Breach, https://books.google.de/books?id=9kSRJaLJ9EEC, 1970.

Chau, J. L., Hoffmann, P., Pedatella, N. M., Matthias, V., and Stober, G.: Upper mesospheric lunar tides over middle and high latitudes during sudden stratospheric warming events, Journal of Geophysical Research: Space Physics, 120, 3084–3096, https://doi.org/10.1002/2015JA020998, https://agupubs.onlinelibrary.wiley.com/doi/abs/10.1002/2015JA020998, 2015.

Chen, C., Chu, X., McDonald, A. J., Vadas, S. L., Yu, Z., Fong, W., and Lu, X.: Inertia-gravity waves in Antarctica: A case study using simultaneous lidar and radar measurements at McMurdo/Scott Base (77.8°S, 166.7°E), Journal of Geophysical Research: Atmospheres, 118, 2794–2808, https://doi.org/10.1002/jgrd.50318, https://agupubs.onlinelibrary.wiley.com/doi/abs/10.1002/jgrd.50318, 2013.

Conte, J. F., Chau, J. L., Stober, G., Pedatella, N., Maute, A., Hoffmann, P., Janches, D., Fritts, D., and Murphy, D. J.: Climatology of semidiurnal lunar and solar tides at middle and high latitudes: Interhemispheric comparison, Journal of Geophysical Research: Space Physics, 122, 7750–7760, https://doi.org/10.1002/2017JA024396, https://agupubs.onlinelibrary.wiley.com/doi/abs/10.1002/2017JA024396, 2017.

Conte, J. F., Chau, J. L., Laskar, F. I., Stober, G., Schmidt, H., and Brown, P.: Semidiurnal solar tide differences between fall and spring transition times in the Northern Hemisphere, Annales Geophysicae, 36, 999–1008, https://doi.org/10.5194/angeo-36-999-2018, https://www.ann-geophys.net/36/999/2018/, 2018.

Coy, L. and Pawson, S.: The Major Stratospheric Sudden Warming of January 2013: Analyses and Forecasts in the GEOS-5 Data Assimilation System, Monthly Weather Review, 143, 491–510, https://doi.org/10.1175/MWR-D-14-00023.1, https://doi.org/10.1175/MWR-D-14-00023.1, 2015.

Davis, R. N., Du, J., Smith, A. K., Ward, W. E., and Mitchell, N. J.: The diurnal and semidiurnal tides over Ascension Island (8° S, 14° W) and their interaction with the stratospheric quasi-biennial oscillation: studies with meteor radar, eCMAM and WACCM, Atmospheric Chemistry and Physics, 13, 9543–9564, https://doi.org/10.5194/acp-13-9543-2013, https://www.atmos-chem-phys.net/13/9543/2013/, 2013.

Dawkins, E. C. M., Feofilov, A., Rezac, L., Kutepov, A. A., Janches, D., Hoeffner, J., Chu, X., Lu, X., Mlynczak, M. G., and Russell, J.: Validation of SABER v2.0 Operational Temperature Data With Ground-Based Lidars in the Mesosphere-Lower Thermosphere Region (75-105 km), Journal of Geophysical Research: Atmospheres, 123, 9916–9934, https://doi.org/10.1029/2018JD028742, https://doi.org/10.1029/2018JD028742, 2018.

Dhadly, M. S., Emmert, J. T., Drob, D. P., McCormack, J. P., and Niciejewski, R. J.: Short-Term and Interannual Variations of Migrating Diurnal and Semidiurnal Tides in the Mesosphere and Lower Thermosphere, Journal of Geophysical Research: Space Physics, 123, 7106–7123, https://doi.org/10.1029/2018JA025748, https://agupubs.onlinelibrary.wiley.com/doi/abs/10.1029/2018JA025748, 2018.

Dörnbrack, A., Pitts, M. C., Poole, L. R., Orsolini, Y. J., Nishii, K., and Nakamura, H.: The 2009–2010 Arctic stratospheric winter – general evolution, mountain waves and predictability of an operational weather forecast model, Atmospheric Chemistry and Physics, 12, 3659–3675, https://doi.org/10.5194/acp-12-3659-2012, https://www.atmos-chem-phys.net/12/3659/2012/, 2012.

Eckermann, S. D., Hoppel, K. W., Coy, L., McCormack, J. P., Siskind, D. E., Nielsen, K., Kochenash, A., Stevens, M. H., Englert, C. R., Singer, W., and Hervig, M.: High-altitude data assimilation system experiments for the northern summer mesosphere season of 2007, Journal of Atmospheric and Solar-Terrestrial Physics, 71, 531 – 551, https://doi.org/https://doi.org/10.1016/j.jastp.2008.09.036, http://www.sciencedirect.com/science/article/pii/S1364682608002575, global Perspectives on the Aeronomy of the Summer Mesopause Region, 2009.

Eckermann, S. D., Ma, J., Hoppel, K. W., Kuhl, D. D., Allen, D. R., Doyle, J. A., Viner, K. C., Ruston, B. C., Baker, N. L., Swadley, S. D., Whitcomb, T. R., Reynolds, C. A., Xu, L., Kaifler, N., Kaifler, B., Reid, I. M., Murphy, D. J., and Love, P. T.: High-Altitude (0-100 km) Global Atmospheric Reanalysis System: Description and Application to the 2014 Austral Winter of the Deep Propagating Gravity Wave Experiment (DEEPWAVE), Monthly Weather Review, 146, 2639–2666, https://doi.org/10.1175/MWR-D-17-0386.1, https://doi.org/10.1175/MWR-D-17-0386.1, 2018.

Ehard, B., Kaifler, B., Kaifler, N., and Rapp, M.: Evaluation of methods for gravity wave extraction from middle-atmospheric lidar temperature measurements, Atmospheric Measurement Techniques, 8, 4645–4655, https://doi.org/10.5194/amt-8-4645-2015, https://www.atmos-meas-tech.net/8/4645/2015/, 2015.

Fejer, B. G., Olson, M. E., Chau, J. L., Stolle, C., Lühr, H., Goncharenko, L. P., Yumoto, K., and Nagatsuma, T.: Lunar-dependent equatorial ionospheric electrodynamic effects during sudden stratospheric warmings, Journal of Geophysical Research: Space Physics, 115, https://doi.org/10.1029/2010JA015273, https://agupubs.onlinelibrary.wiley.com/doi/abs/10.1029/2010JA015273, 2010.

Forbes, J. M.: Atmospheric tides: 1. Model description and results for the solar diurnal component, Journal of Geophysical Research: Space Physics, 87, 5222–5240, https://doi.org/10.1029/JA087iA07p05222, https://agupubs.onlinelibrary.wiley.com/doi/abs/10.1029/JA087iA07p05222, 1982.

Forbes, J. M. and Zhang, X.: Lunar tide amplification during the January 2009 stratosphere warming event: Observations and theory, Journal of Geophysical Research: Space Physics, 117, https://doi.org/10.1029/2012JA017963, https://agupubs.onlinelibrary.wiley.com/doi/abs/10.1029/2012JA017963, 2012.

Forbes, J. M., Zhang, X., Palo, S., Russell, J., Mertens, C. J., and Mlynczak, M.: Tidal variability in the ionospheric dynamo region, Journal of Geophysical Research: Space Physics, 113, https://doi.org/10.1029/2007JA012737, https://agupubs.onlinelibrary.wiley.com/doi/abs/10.1029/2007JA012737, 2008.

Fricke-Begemann, C., Alpers, M., and Höffner, J.: Daylight rejection with a new receiver for potassium resonance temperature lidars, Opt. Lett., 27, 1932–1934, https://doi.org/10.1364/OL.27.001932, http://ol.osa.org/abstract.cfm?URI=ol-27-21-1932, 2002.

Fritts, D. C., Miller, A. D., Kjellstrand, C. B., Geach, C., Williams, B. P., Kaifler, B., Kaifler, N., Jones, G., Rapp, M., Limon, M., Reimuller, J., Wang, L., Hanany, S., Gisinger, S., Zhao, Y., Stober, G., and Randall, C. E.: PMC Turbo: Studying Gravity Wave and Instability Dynamics in the Summer Mesosphere Using Polar Mesospheric Cloud Imaging and Profiling From a Stratospheric Balloon, Journal of Geophysical Research: Atmospheres, 124, 6423–6443, https://doi.org/10.1029/2019JD030298, https://agupubs.onlinelibrary.wiley.com/doi/abs/10.1029/2019JD030298, 2019.

Fuller-Rowell, T., Wu, F., Akmaev, R., Fang, T.-W., and Araujo-Pradere, E.: A whole atmosphere model simulation of the impact of a sudden stratospheric warming on thermosphere dynamics and electrodynamics, Journal of Geophysical Research: Space Physics, 115, https://doi.org/10.1029/2010JA015524, https://agupubs.onlinelibrary.wiley.com/doi/abs/10.1029/2010JA015524, 2010.

Fuller-Rowell, T. J., Fang, T.-W., Wang, H., Matthias, V., Hoffmann, P., Hocke, K., and Studer, S.: Impact of Migrating Tides on Electrodynamics During the January 2009 Sudden Stratospheric Warming, chap. 14, pp. 163–174, American Geophysical Union (AGU), https://doi.org/10.1002/9781118929216.ch14, https://agupubs.onlinelibrary.wiley.com/doi/abs/10.1002/9781118929216.ch14, 2016.

Gerding, M., Höffner, J., Lautenbach, J., Rauthe, M., and Lübken, F.-J.: Seasonal variation of nocturnal temperatures between 1 and 105 km altitude at 54° N observed by lidar, Atmospheric Chemistry and Physics, 8, 7465–7482, https://doi.org/10.5194/acp-8-7465-2008, https://www.atmos-chem-phys.net/8/7465/2008/, 2008.

Hauchecorne, A. and Chanin, M. L.: Density and Temperature Profiles obtained by Lidar between 35 and 70 km, Geophys. Res. Lett., 7, 565–568, 1980.

He, M., Chau, J. L., Stober, G., Li, G., Ning, B., and Hoffmann, P.: Relations Between Semidiurnal Tidal Variants Through Diagnosing the Zonal Wavenumber Using a Phase Differencing Technique Based on Two Ground-Based Detectors, Journal of Geophysical Research: Atmospheres, 123, 4015–4026, https://doi.org/10.1002/2018JD028400, https://agupubs.onlinelibrary.wiley.com/doi/abs/10.1002/2018JD028400, 2018.

Hocking, W., Fuller, B., and Vandepeer, B.: Real-time determination of meteor-related parameters utilizing modern digital technology, Journal of Atmospheric and Solar-Terrestrial Physics, 63, 155 – 169, https://doi.org/http://dx.doi.org/10.1016/S1364-6826(00)00138-3, http://www.sciencedirect.com/science/article/pii/S1364682600001383, radar applications for atmosphere and ionosphere research - PIERS 1999, 2001.

Hogan, T. F., Liu, M., Ridout, J. A., Peng, M. S., Whitcomb, T. R., Ruston, B. C., Reynolds, C. A., Eckermann, S. D., Moskaitis, J. R., Baker, N. L., McCormack, J. P., Viner, K. C., McLay, J. G., Flatau, M. K., Xu, L., Chen, C., and Chang, S. W.: The Navy Global Environmental Model, Oceanography, 27, https://doi.org/10.5670/oceanog.2014.73, 2014.

Jacobi, C., Hoffmann, P., and Kürschner, D.: Trends in MLT region winds and planetary waves, Collm (52° N, 15° E), Annales Geophysicae, 26, 1221–1232, https://doi.org/10.5194/angeo-26-1221-2008, https://www.ann-geophys.net/26/1221/2008/, 2008.

Jin, H., Miyoshi, Y., Pancheva, D., Mukhtarov, P., Fujiwara, H., and Shinagawa, H.: Response of migrating tides to the stratospheric sudden warming in 2009 and their effects on the ionosphere studied by a whole atmosphere-ionosphere model GAIA with COSMIC and TIMED/SABER observations, Journal of Geophysical Research: Space Physics, 117, https://doi.org/10.1029/2012JA017650, https://agupubs.onlinelibrary.wiley.com/doi/abs/10.1029/2012JA017650, 2012.

Jones Jr., M., Drob, D. P., Siskind, D. E., McCormack, J. P., Maute, A., McDonald, S. E., and Dymond, K. F.: Evaluating Different Techniques for Constraining Lower Atmospheric Variability in an Upper Atmosphere General Circulation Model: A Case Study During the 2010 Sudden Stratospheric Warming, Journal of Advances in Modeling Earth Systems, 10, 3076–3102, https://doi.org/10.1029/2018MS001440, https://agupubs.onlinelibrary.wiley.com/doi/abs/10.1029/2018MS001440, 2018.

Kuhl, D., Rosmond, T., Bishop, C., McLay, J., and Baker, N.: Comparison of hybrid ensemble/4DVar and 4DVar within the NAVDAS-AR data assimilation framework, Mon. Wea. Rev., 141, 2740–2758, https://doi.org/10.1175/MWR-D-12-00182.1, 2013.

Laskar, F. I., McCormack, J. P., Chau, J. L., Pallamraju, D., Hoffmann, P., and Singh, R. P.: Interhemispheric Meridional Circulation During Sudden Stratospheric Warming, Journal of Geophysical Research: Space Physics, 124, 7112–7122, https://doi.org/10.1029/2018JA026424, https://agupubs.onlinelibrary.wiley.com/doi/abs/10.1029/2018JA026424, 2019.

Lima, L. M., Paulino, A. R. S., Medeiros, A. F., Buriti, R. A., Batista, P. P., Clemesha, B. R., and Takahashi, H.: First observation of the diurnal and semidiurnal ocillation in the mesospheric winds over São João do Cariri-PB, Brazil, Revista Brasileira de Geofísica, 25, 35–41, http://www.scielo.br/scielo.php?script=sci_arttext&pid=S0102-261X2007000600005&nrm=iso, 2007.

Limpasuvan, V., Orsolini, Y. J., Chandran, A., Garcia, R. R., and Smith, A. K.: On the composite response of the MLT to major sudden stratospheric warming events with elevated stratopause, Journal of Geophysical Research: Atmospheres, 121, 4518–4537, https://doi.org/10.1002/2015JD024401, https://agupubs.onlinelibrary.wiley.com/doi/abs/10.1002/2015JD024401, 2016.

Lindzen, R. S.: Atmospheric Tides, Annual Review of Earth and Planetary Sciences, 7, 199–225, https://doi.org/10.1146/annurev.ea.07.050179.001215, https://doi.org/10.1146/annurev.ea.07.050179.001215, 1979.

Liu, H., Miyoshi, Y., Miyahara, S., Jin, H., Fujiwara, H., and Shinagawa, H.: Thermal and dynamical changes of the zonal mean state of the thermosphere during the 2009 SSW: GAIA simulations, Journal of Geophysical Research: Space Physics, 119, 6784–6791, https://doi.org/10.1002/2014JA020222, https://agupubs.onlinelibrary.wiley.com/doi/abs/10.1002/2014JA020222, 2014.

Liu, H.-L.: Variability and predictability of the space environment as related to lower atmosphere forcing, Space Weather, 14, 634–658, https://doi.org/10.1002/2016SW001450, https://agupubs.onlinelibrary.wiley.com/doi/abs/10.1002/2016SW001450, 2016.

Liu, H.-L., Wang, W., Richmond, A. D., and Roble, R. G.: Ionospheric variability due to planetary waves and tides for solar minimum conditions, Journal of Geophysical Research: Space Physics, 115, https://doi.org/10.1029/2009JA015188, https://agupubs.onlinelibrary.wiley.com/doi/abs/10.1029/2009JA015188, 2010.

Lomb, N. R.: Least-squares frequency analysis of unequally spaced data, Astrophysics and Space Science, 39, 447–462, https://doi.org/10.1007/BF00648343, http://dx.doi.org/10.1007/BF00648343, 1976.

Manney, G. L., Krüger, K., Pawson, S., Minschwaner, K., Schwartz, M. J., Daffer, W. H., Livesey, N. J., Mlynczak, M. G., Remsberg, E. E., Russell III, J. M., and Waters, J. W.: The evolution of the stratopause during the 2006 major warming: Satellite data and assimilated meteorological analyses, Journal of Geophysical Research: Atmospheres, 113, https://doi.org/10.1029/2007JD009097, https://agupubs.onlinelibrary.wiley.com/doi/abs/10.1029/2007JD009097, 2008.

Manney, G. L., Schwartz, M. J., Krüger, K., Santee, M. L., Pawson, S., Lee, J. N., Daffer, W. H., Fuller, R. A., and Livesey, N. J.: Aura Microwave Limb Sounder observations of dynamics and transport during the record-breaking 2009 Arctic stratospheric major warming, Geophysical Research Letters, 36, https://doi.org/10.1029/2009GL038586, https://agupubs.onlinelibrary.wiley.com/doi/abs/10.1029/2009GL038586, 2009.

Marsh, D. R.: Chemical–Dynamical Coupling in the Mesosphere and Lower Thermosphere, pp. 3–17, Springer Netherlands, Dordrecht, https://doi.org/10.1007/978-94-007-0326-1_1, https://doi.org/10.1007/978-94-007-0326-1_1, 2011.

Matsuno, T.: A Dynamical Model of the Stratospheric Sudden Warming, Journal of the Atmospheric Sciences, 28, 1479–1494, https://doi.org/10.1175/1520-0469(1971)028<1479:ADMOTS>2.0.CO;2, https://doi.org/10.1175/1520-0469(1971)028<1479:ADMOTS>2.0.CO;2, 1971.

Matthias, V., Hoffmann, P., Rapp, M., and Baumgarten, G.: Composite analysis of the temporal development of waves in the polar {MLT} region during stratospheric warmings, Journal of Atmospheric and Solar-Terrestrial Physics, 90 - 91, 86 – 96, https://doi.org/http://dx.doi.org/10.1016/j.jastp.2012.04.004, recent Progress in the Vertical Coupling in the Atmosphere-Ionosphere System, 2012.

Matthias, V., Hoffmann, P., Manson, A., Meek, C., Stober, G., Brown, P., and Rapp, M.: The impact of planetary waves on the latitudinal displacement of sudden stratospheric warmings, Annales Geophysicae, 31, 1397–1415, https://doi.org/10.5194/angeo-31-1397-2013, http://www.ann-geophys.net/31/1397/2013/, 2013.

McCormack, J., Hoppel, K., Kuhl, D., de Wit, R., Stober, G., Espy, P., Baker, N., Brown, P., Fritts, D., Jacobi, C., Janches, D., Mitchell, N., Ruston, B., Swadley, S., Viner, K., Whitcomb, T., and Hibbins, R.: Comparison of mesospheric winds from a high-altitude meteorological analysis system and meteor radar observations during the boreal winters of 2009-2010 and 2012-2013, Journal of Atmospheric and Solar-Terrestrial Physics, 154, 132 – 166, https://doi.org/http://dx.doi.org/10.1016/j.jastp.2016.12.007, http://www.sciencedirect.com/science/article/pii/S1364682616303182, 2017.

McCormack, J. P., Eckermann, S. D., and Hogan, T. F.: Generation of a Quasi-Biennial Oscillation in an NWP Model Using a Stochastic Gravity Wave Drag Parameterization, Monthly Weather Review, 143, 2121–2147, https://doi.org/10.1175/MWR-D-14-00208.1, https://doi.org/10.1175/MWR-D-14-00208.1, 2015.

Merzlyakov, E., Jacobi, C., Portnyagin, Y., and Solovjova, T.: Structural changes in trend parameters of the MLT winds based on wind measurements at Obninsk (55°N, 37°E) and Collm (52°N, 15°E), J. of Atmospheric and Solar-Terrestrial Physics, 71, 1547–1557, https://doi.org/https://doi.org/10.1016/j.jastp.2009.05.013, http://www.sciencedirect.com/science/article/pii/S1364682609001461, long-Term Changes and Trends in the Atmosphere-Ionosphere System, 2009.

Miyoshi, Y., Pancheva, D., Mukhtarov, P., Jin, H., Fujiwara, H., and Shinagawa, H.: Excitation mechanism of non-migrating tides, J. of Atmospheric and Solar-Terrestrial Physics, 156, 24–36, https://doi.org/https://doi.org/10.1016/j.jastp.2017.02.012, http://www.sciencedirect.com/science/article/pii/S1364682616302711, 2017.

Oberheide, J., Forbes, J. M., Häusler, K., Wu, Q., and Bruinsma, S. L.: Tropospheric tides from 80 to 400 km: Propagation, interannual variability, and solar cycle effects, Journal of Geophysical Research: Atmospheres, 114, https://doi.org/10.1029/2009JD012388, https://agupubs.onlinelibrary.wiley.com/doi/abs/10.1029/2009JD012388, 2009.

Oberheide, J., Forbes, J. M., Zhang, X., and Bruinsma, S. L.: Climatology of upward propagating diurnal and semidiurnal tides in the thermosphere, Journal of Geophysical Research: Space Physics, 116, https://doi.org/10.1029/2011JA016784, https://agupubs.onlinelibrary.wiley.com/doi/abs/10.1029/2011JA016784, 2011.

Pedatella, N. M. and Forbes, J. M.: Evidence for stratosphere sudden warming-ionosphere coupling due to vertically propagating tides, Geophysical Research Letters, 37, https://doi.org/10.1029/2010GL043560, https://agupubs.onlinelibrary.wiley.com/doi/abs/10.1029/2010GL043560, 2010.

Pedatella, N. M. and Maute, A.: Impact of the semidiurnal lunar tide on the midlatitude thermospheric wind and ionosphere during sudden stratosphere warmings, Journal of Geophysical Research: Space Physics, 120, 10,740–10,753, https://doi.org/10.1002/2015JA021986, https://agupubs.onlinelibrary.wiley.com/doi/abs/10.1002/2015JA021986, 2015.

Pedatella, N. M., Liu, H.-L., and Richmond, A. D.: Atmospheric semidiurnal lunar tide climatology simulated by the Whole Atmosphere Community Climate Model, Journal of Geophysical Research: Space Physics, 117, https://doi.org/10.1029/2012JA017792, https://agupubs.onlinelibrary.wiley.com/doi/abs/10.1029/2012JA017792, 2012.

Pedatella, N. M., Fuller-Rowell, T., Wang, H., Jin, H., Miyoshi, Y., Fujiwara, H., Shinagawa, H., Liu, H.-L., Sassi, F., Schmidt, H., Matthias, V., and Goncharenko, L.: The neutral dynamics during the 2009 sudden stratosphere warming simulated by different whole atmosphere models, Journal of Geophysical Research: Space Physics, 119, 1306–1324, https://doi.org/10.1002/2013JA019421, https://agupubs.onlinelibrary.wiley.com/doi/abs/10.1002/2013JA019421, 2014.

Pokhotelov, D., Becker, E., Stober, G., and Chau, J. L.: Seasonal variability of atmospheric tides in the mesosphere and lower thermosphere: meteor radar data and simulations, Annales Geophysicae, 36, 825–830, https://doi.org/10.5194/angeo-36-825-2018, https://www.ann-geophys.net/36/825/2018/, 2018.

Portnyagin, Y., Forbes, J., Fraser, G., Vlncent, R., Avery, S., Lysenko, I., and Makarov, N.: Dynamics of the Antarctic and Arctic mesosphere and lower thermosphere regions II. The semidiurnal tide, J. of Atmospheric and Terrestrial Physics, 55, 843–855, https://doi.org/https://doi.org/10.1016/0021-9169(93)90025-T, http://www.sciencedirect.com/science/article/pii/002191699390025T, 1993.

Portnyagin, Y. I., Solovjova, T. V., Makarov, N. A., Merzlyakov, E. G., Manson, A. H., Meek, C. E., Hocking, W., Mitchell, N., Pancheva, D., Hoffmann, P., Singer, W., Murayama, Y., Igarashi, K., Forbes, J. M., Palo, S., Hall, C., and Nozawa, S.: Monthly mean climatology of the prevailing winds and tides in the Arctic mesosphere/lower thermosphere, Annales Geophysicae, 22, 3395–3410, https://doi.org/10.5194/angeo-22-3395-2004, https://www.ann-geophys.net/22/3395/2004/, 2004.

Rüfenacht, R., Baumgarten, G., Hildebrand, J., Schranz, F., Matthias, V., Stober, G., Lübken, F.-J., and Kämpfer, N.: Intercomparison of middle-atmospheric wind in observations and models, Atmospheric Measurement Techniques, 11, 1971–1987, https://doi.org/10.5194/amt-11-1971-2018, https://www.atmos-meas-tech.net/11/1971/2018/, 2018.

Sandford, D. J., Muller, H. G., and Mitchell, N. J.: Observations of lunar tides in the mesosphere and lower thermosphere at Arctic and middle latitudes, Atmospheric Chemistry and Physics, 6, 4117–4127, https://doi.org/10.5194/acp-6-4117-2006, https://www.atmos-chem-phys.net/6/4117/2006/, 2006.

Scargle, J. D.: Studies in astronomical time series analysis. II - Statistical aspects of spectral analysis of unevenly spaced data, Astrophysical Journal, 263, 835–853, 1982.

Schranz, F., Hagen, J., Stober, G., Hocke, K., Murk, A., and Kämpfer, N.: Small-scale variability of stratospheric ozone during the SSW 2018/2019 observed at Ny-Ålesund, Svalbard, Atmospheric Chemistry and Physics Discussions, 2019, 1–25, https://doi.org/10.5194/acp-2019-1093, https://www.atmos-chem-phys-discuss.net/acp-2019-1093/, 2019.

Schwartz, M., Lambert, A., Manney, G., Read, W., Livesey, N., Froidevaux, L., Ao, C., Bernath, P., Boone, C., Cofield, R., Daffer, W., Drouin, B., Fetzer, E., Fuller, R., Jarnot, R., Jiang, J., Jiang, Y., Knosp, B. W., Krüger, K., Li, J.-L., Mlynczak, M., Pawson, S., Russell, J., Santee, M., Snyder, W., Stek, P., Thurstans, R., Tompkins, A., Wagner, P., Walker, K., Waters, J. W., and Wu, D. L.: Validation of the

Aura Microwave Limb Sounder temperature and geopotential height measurements, Journal of Geophysical Research: Atmospheres, 113, https://doi.org/10.1029/2007JD008783, http://dx.doi.org/10.1029/2007JD008783, d15S11, 2008.

Shibuya, R., Sato, K., Tsutsumi, M., Sato, T., Tomikawa, Y., Nishimura, K., and Kohma, M.: Quasi-12 h inertia–gravity waves in the lower mesosphere observed by the PANSY radar at Syowa Station (39.6° E, 69.0° S), Atmospheric Chemistry and Physics, 17, 6455–6476, https://doi.org/10.5194/acp-17-6455-2017, https://www.atmos-chem-phys.net/17/6455/2017/, 2017.

Siddiqui, T. A., Yamazaki, Y., Stolle, C., Lühr, H., Matzka, J., Maute, A., and Pedatella, N.: Dependence of Lunar Tide of the Equatorial Electrojet on the Wintertime Polar Vortex, Solar Flux, and QBO, Geophysical Research Letters, 45, 3801–3810, https://doi.org/10.1029/2018GL077510, https://agupubs.onlinelibrary.wiley.com/doi/abs/10.1029/2018GL077510, 2018.

Smith, A. K.: Global Dynamics of the MLT, Surveys in Geophysics, 33, 1177–1230, https://doi.org/10.1007/s10712-012-9196-9, https://doi.org/10.1007/s10712-012-9196-9, 2012.

Stober, G., Latteck, R., Rapp, M., Singer, W., and Zecha, M.: MAARSY - the new MST radar on Andøya: first results of spaced antenna and Doppler measurements of atmospheric winds in the troposphere and mesosphere using a partial array, Advances in Radio Science, 10, 291–298, https://doi.org/10.5194/ars-10-291-2012, http://www.adv-radio-sci.net/10/291/2012/, 2012.

Stober, G., Matthias, V., Jacobi, C., Wilhelm, S., Höffner, J., and Chau, J. L.: Exceptionally strong summer-like zonal wind reversal in the upper mesosphere during winter 2015/16, Annales Geophysicae, 35, 711–720, https://doi.org/10.5194/angeo-35-711-2017, https://www.ann-geophys.net/35/711/2017/, 2017.

Stober, G., Chau, J. L., Vierinen, J., Jacobi, C., and Wilhelm, S.: Retrieving horizontally resolved wind fields using multi-static meteor radar observations, Atmospheric Measurement Techniques, 11, 4891–4907, https://doi.org/10.5194/amt-11-4891-2018, https://www.atmos-meas-tech.net/11/4891/2018/, 2018.

Stockwell, R. G., Mansinha, L., and Lowe, R. P.: Localization of the complex spectrum: the S transform, IEEE Transactions on Signal Processing, 44, 998–1001, https://doi.org/10.1109/78.492555, 1996.

Stray, N. H., Orsolini, Y. J., Espy, P. J., Limpasuvan, V., and Hibbins, R. E.: Observations of planetary waves in the mesosphere-lower thermosphere during stratospheric warming events, Atmospheric Chemistry and Physics, 15, 4997–5005, https://doi.org/10.5194/acp-15-4997-2015, https://www.atmos-chem-phys.net/15/4997/2015/, 2015.

Torrence, C. and Compo, G. P.: A Practical Guide to Wavelet Analysis, Bull. Amer. Meteor. Soc., 79, 61–78, 1998.

von Zahn, U. and Höffner, J.: Mesopause temperature profiling by potassium lidar, Geophysical Research Letters, 23, 141–144, https://doi.org/10.1029/95GL03688, https://agupubs.onlinelibrary.wiley.com/doi/abs/10.1029/95GL03688, 1996.

Wang, H., Boyd, J. P., and Akmaev, R. A.: On computation of Hough functions, Geoscientific Model Development, 9, 1477–1488, https://doi.org/10.5194/gmd-9-1477-2016, https://www.geosci-model-dev.net/9/1477/2016/, 2016.

Wilhelm, S., Stober, G., and Chau, J. L.: A comparison of 11-year mesospheric and lower thermospheric winds determined by meteor and MF radar at 69° N, Annales Geophysicae, 35, 893–906, https://doi.org/10.5194/angeo-35-893-2017, https://www.ann-geophys.net/35/893/2017/, 2017.

Wilhelm, S., Stober, G., and Brown, P.: Climatologies and long-term changes in mesospheric wind and wave measurements based on radar observations at high and mid latitudes, Annales Geophysicae, 37, 851–875, https://doi.org/10.5194/angeo-37-851-2019, https://www.ann-geophys.net/37/851/2019/, 2019.

Xu, F. and San Liang, X.: On the Generation and Maintenance of the 2012/13 Sudden Stratospheric Warming, Journal of the Atmospheric Sciences, 74, 3209–3228, https://doi.org/10.1175/JAS-D-17-0002.1, https://doi.org/10.1175/JAS-D-17-0002.1, 2017.

Xu, J., She, C. Y., Yuan, W., Mertens, C., Mlynczak, M., and Russell, J.: Comparison between the temperature measurements by TIMED/SABER and lidar in the midlatitude, Journal of Geophysical Research: Space Physics (1978–2012), 111, https://doi.org/10.1029/2005JA011439, https://doi.org/10.1029/2005JA011439, 2006.

Yu, Y., Wan, W., Ning, B., Liu, L., Wang, Z., Hu, L., and Ren, Z.: Tidal wind mapping from observations of a meteor radar chain in December 2011, Journal of Geophysical Research: Space Physics, 118, 2321–2332, https://doi.org/10.1029/2012JA017976, https://agupubs.onlinelibrary.wiley.com/doi/abs/10.1029/2012JA017976, 2013.

Zhang, X., Forbes, J. M., Hagan, M. E., Russell III, J. M., Palo, S. E., Mertens, C. J., and Mlynczak, M. G.: Monthly tidal temperatures 20–120 km from TIMED/SABER, Journal of Geophysical Research: Space Physics, 111, https://doi.org/10.1029/2005JA011504, https://agupubs.onlinelibrary.wiley.com/doi/abs/10.1029/2005JA011504, 2006.

Zülicke, C., Becker, E., Matthias, V., Peters, D. H. W., Schmidt, H., Liu, H.-L., Ramos, L. d. l. T., and Mitchell, D. M.: Coupling of Stratospheric Warmings with Mesospheric Coolings in Observations and Simulations, Journal of Climate, 31, 1107–1133, https://doi.org/10.1175/JCLI-D-17-0047.1, https://doi.org/10.1175/JCLI-D-17-0047.1, 2018.